UNIVERSITY OF NAPLES FEDERICO II

Department of Chemical, Materials, and Industrial Production Engineering

Ph.D COURSE IN CHEMICAL ENGENEERING

XXVI CYCLE

" DEVELOPMENT AND FABRICATION OF MICROFLUIDIC DEVICES TO CONTROL CELL MICROENVIRONMENT"

Scientific Committee:

Prof. Pier Luca Maffettone

Prof. Paolo Antonio Netti

Prof. Maurizio Ventre

Dott. Francesco Greco

Candidate:

Gemma Pagano

March 2011- March 2014

To my family

Acknowledgments

Foremost, I would like to express my deepest gratitude to Prof. P.A. Netti, Prof. P.L. Maffettone and Dr. F. Greco for their valuable support and precious guidance and for giving me the opportunity to work on this project.

My sincere thanks also goes to Prof. M. Swartz for giving me the internship opportunities in her group and letting me work on an exciting project.

This thesis would not have been possible without the help, scientific support and patience of Prof. M. Ventre and Dr. M. Iannone. I owe much of my knowledge, expertise and maturity to them.

I would like to thank my fantastic family, the only reference of my life, their never-ending support gives me the confidence to keep setting goals for myself.

I am most grateful to my grandmother and Gigi, their teachings and their constant stimuli were decisive for my growth.

I would like to thank my boyfriend, Domenico, who has always brightened my days and has given me unconditional support tolerating my constant mood swings. His absence when I was in Lausanne made me understand how much he is part of me.

A very special thanks goes to Gabriella, my all time friend, I shared everything with her. My international experience would not have been the same without her long and funny skype calls. I am very lucky to have met her in my life.

I would like to sincerely thank Ilaria e Giovanna for constant encouragement under all circumstances.

Many thanks go to my fellow colleagues: Annabella, Lucia, Alessandra, Carlo, David, Costantino, Virginia and Alessandro for all the support they have showered on me.

I would also like to thank Enza, my first grad student, I spent several happy days in the laboratory with her.

Finally, I thank Marco and all those who extended their helping hands towards me in various ways during my internship in Lausanne.

Table of Contents

Chapter 1……7

Introduction……7

1.1 Cell Microenviroment……...7

1.2 Biochemical Signals……..9

1.3 Mechanical Signals: Interstitial Fluid Flow……..9

1.4 Interaction of Biochemical and Mechanical Signals……..…11

1.5 Microfluidics to Control Cell Microenvironment……...13

1.6 Microfluidic Devices as Gradient Generetors……16

1.7 Aims of Thesis……20

1.8 References……...21

Chapter 2…… 25

Development and Fabrication of a Microfluidic Device for Generating Stable Concentration Gradient in 3D environment…….25

2.1 Materials and Methods……....27

Design of Microfluidic Device……...27

Computation Fluid Dynamics (CFD) and Transport Modeling……..28

Fabrication and Assembly of Microfluidic Device……28

3D Gel Preparation and Filling……...29

Gradient Profile Characterization……...30

Cell Culture and Chemotaxis Experiment……..31

Data Analysis……..32

2.2 Results and Discussion……..32

Numerical simulation……..32

Optimization of Gel-Wall Attachment……34

Gas Bubbles in the Gel Matrix……35

Gas Bubbles in the Side Channels……..37

Gradient Characterization……39

hMSC Migration in Response to BMP-2 Gradients.....40

2.3 Conclusion 44

2.4 References 45

Chapter 3…… 47

Effects of interstitial flow on collective tumor cell invasion in a 3D model system……...47

3.1 Materials and Methods……49

Cell Culture……..49

3D Spheroid Formation……49

Radial Flow Chamber Assembly…….50

Estimation of the Flow Field in the Flow Chamber…….51

Spheroid Sprouting Experiment and Quantification……52

3.2 Results.....53

Computational estimation of the interstitial flow field in the matrix……...53

Interstitial flow decreases 4T-1 cell sprouting…….....54

3.3 Conclusion……..57

3.4 References……...58

Chapter 4…… 61

4.1 Overall Conclusions...…….....……...61

4.2 Future Directions……62

Chapter 1

Introduction

In vivo cell behaviour is regulated by a cascade of biological stimulation that are finely delivered to the extracellular environment.

The environmental stimulation includes interactions with other cells, interactions with the extracellular matrix, and systemic factors (e.g. hormones). These signals, often presenting themselves to cells according to specific temporal and spatial programmes, drive cellular behaviours and function during development and tissue regeneration [1].

The ability to change and control the microenvironment and the spatial location of their signals may better facilitate the capacity to regulate cell fate and even to recapitulate gradients present during normal physiologic processes to permit regional control of cell function for the design of cell based therapies for use in regenerative medicine [2,3]. Eben Alsberg, an associate professor of biomedical engineering and orthopaedic surgery at Case Western Reserve said: "If we can control the spatial presentation of signals, we may be able to have more control over cell behavior and enhance the rate and quality of tissue formation". Therefore in order to obtain functional tissues it is necessary to control the presentation of signals within defined microenvironment to elicit a given and predefined cell response. *In vivo* the investigation of stimulant-specific cellular events is technically difficult because many signals act synergistically but the development of reliable and consistent *in vitro* platform is the starting point to capture the logic behind signal presentation. Micronscale platforms provide an unique tool to investigate how physical and biochemical signals or their combination can guide cells in many biological process in a precise manner [4].

1.1 Cell Microenvironment

In vivo, cells reside in a complex and organized environment with a very specific 3D extracellular matrix (ECM), which provides an essential physical scaffolding for the cellular constituents. The ECM is a highly hydrated, viscoelastic three-dimensional (3D) network containing structural proteins (e.g. collagens, elastins), adhesive proteins (e.g. fibronectin, laminins), and ground substance (primarily glycosaminoglycans, proteoglycans, and other

glycoproteins) [5]. Most of cells type are embedded in the ECM. Within this environment cells interact with other cells (cell-cell contacts), or with the matrix (cell-matrix interactions). Additionally, cells are constantly exposed to chemical factors (e.g. cytokines, growth factors, hormones), mechanical and physiochemical stimuli (e.g. interstitial fluid flow, shear stress, pressure or compression, oxygen tension, pH, temperature). These act continuously and simultaneously and they are presented to the cells in the form of spatio-temporal variations of concentration, stiffness, density, and other properties rather than in an on/off like manner. Therefore, the ECM contains array of signals to control cell behavior. However, cells can also alter the physical-chemical characteristics of the ECM thus modifying the information. The combination of all these factors and the complex interplay between cells and their environment influences cellular fate processes and constitutes the *cell microenvironment* (Fig1). For stem cells, the local microenvironment, or stem cell niche, holds the key to regulating stem cell survival, self-renewal, and differentiation [6]. In cancer biology, the tumor microenvironment is also suggested as an important and even necessary component to the progression of some types of cancer.

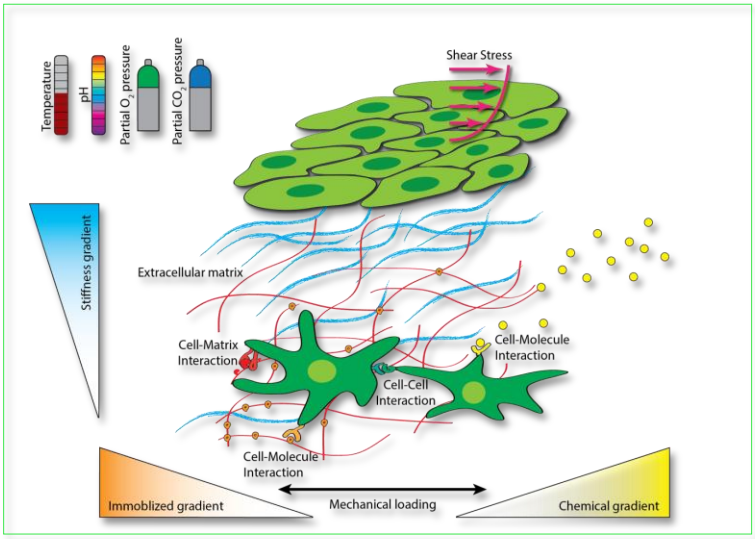

Figure 1.Schematic of cell microenvironment.

1.2 Biochemical Signals

The cell microenvironment includes insoluble and soluble biochemical molecules. The insoluble components are comprised of ECM molecules that form 2D substrates as well as a 3D environment within which cells reside. The soluble signaling molecules include hormones, cytokines and growth factors secreted by local (paracrine signals) or distant (endocrine signals) cells. These molecules are transported away from the source via diffusion. Target cells perceive the extracellular signals predominantly through their surface receptor proteins and then activate complex intracellular biochemical cascades to regulate the cell physiological behaviors. The effects of soluble factors on cell regulation depend on the concentration, half life, and receptor binding affinities of the ligand of interest. However not only the concentration but also the spatial and temporal distribution of these soluble factors is important in regulating cell response. In fact, gradients of biochemical/biophysical signals are found in diverse biological contexts. In more details, biochemical gradients exist naturally due to diffusion, whereas gradients in matrix stiffness or ECM composition are intrinsically built into the heterogeneity of the tissue structure.

Biomolecular gradients play essential roles in many phenomena including development, inflammation, wound healing, and cancer. During the inflammation the biomolecular gradients provide to immune cells the directional cues they need to rapidly migrate to the infection site [7]. In the development of cancer an oxygen concentration gradient, with the highest concentration at the edge of the tumour body, drives the tumour cells to invade other tissue and to promote sprouting of new blood vessels, an important hallmark of tumor progression [8,9]. In each case, chemoattractant-induced activation of spatially localized cellular signals causes cells to polarise and move toward the highest concentration of chemoattractant.

1.3 Mechanical Signals: Interstitial Fluid Flow

The interstitial fluid originates from blood vessel and flows through tridimensional ECM and around cells. The interstitial fluid flow differs from blood flow within vessels for three reasons: 1) it has a velocity much slower due to high flow resistance of extracellular matrix; 2) it moves around the cell-matrix interface in all directions; 3) it can act to bias and amplify the distribution of cell-secreted proteins, creating directional transcellular gradients. The driving force is the

pressure difference between blood and lymphatic vessel and controlled by the flow resistance of the fibrillar matrix (fig.2) [10].

The interstitial fluid flow can be quantified with fluorescence recovery after photobleaching (FRAP) or nuclear magnetic resonance (NMR). Fluid flow through 3D matrices is usually estimated using Darcy's law:

$$v = -\frac{K}{\mu\Phi}\nabla P$$

where v is the pore velocity, μ is dynamic viscosity of interstitial fluid, K is the hydraulic permeability of tissue, Φ is the porosity of tissue and P is the tissue interstitial fluid pressure. In normal tissue the interstitial flow rate varies between 0.1 and 2.0 μm/s [11] but these values can increase to the value of 4 μm/s in presence of inflammation tissue such as solid tumours [12]. In fact during the tumour growth, fluid flow promotes formation of new blood vessels within and around the tumour mass, owing to the permeability of neo-vessel. Furthermore, the abnormal lymphatic vessels sustain this process by increasing the interstitial fluid pressure and flow. In solid tumour the interstitial pressure ranges from 10 mmHg to 20 mmHg while in normal tissue it is < 10 mmHg [13]. This difference in pressure between normal and tumour tissue causes a high interstitial fluid pressure gradients at tumou margin that results in a increase of the magnitude of interstitial flow velocity.

Interstitial fluid flow plays an important role in tissue morphogenesis, cell migration, cell differentiation and matrix remodeling. The mechanism by which such flow can influence cell response might be mechanical, such as shear stress on cell surface[14], or drag forces on the matrix component (which can transmit stress to cells through integrin attachments)[15]. Several studies reported the influence of interstitial flow on cell morphology in literature. For example Ng et al. have observed that human dermal fibroblasts aligned perpendicular to the direction of interstitial flow. In contrast, fibroblasts in static three-dimensional controls remained randomly oriented, whereas cells subjected to fluid shear as a two-dimensional monolayer regressed [16]. The same group demonstrated that low levels of interstitial flow induce fibroblast-to-myofibroblast differentiation as well as collagen alignment and fibroblast proliferation, even in the absence of exogenous mediators [17]. Wang et al. developed a 3D collagen gel model to

simulate interstitial fluid flow and to assess its influence on the biosynthesis of cytokines in smooth muscle cells [18]. Moreover it has been observed a synergistic enhancement of tumor cell invasion by fibroblasts in the presence of interstitial flow. In particular, without interstitial flow, fibroblasts did not affect melanoma cell invasion, while in the presence of interstitial fluid flow the levels of tumor cell invasion increased, through increased TGF-b1 activation and collagen degradation [19].

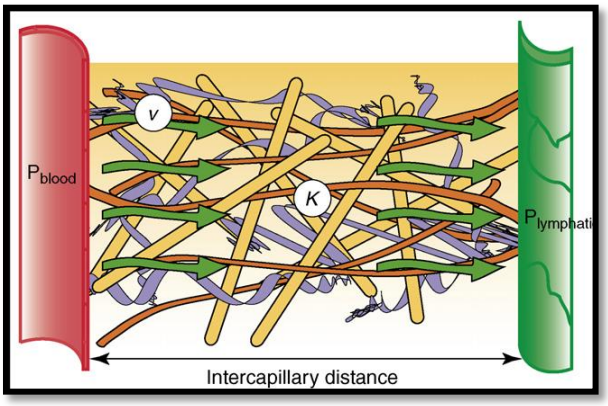

Figure 2. Interstitial fluid flow across 3D matrix.

1.4 Interaction of Biochemical and Mechanical Signals

The interaction between biophysical and biochemical factors are gaining large attention since the regulation of multiple stimulation is key central in various contexts. In particular, the successful implementation of tissue engineering products relies on the long-term performance and stability of tissue constructs which are subjected to diverse signals acting synergistically [20,21]. For instance, during angiogenesis (formation of new blood vessels) a number of angiogenic proteins, including vascular endothelial growth factor (VEGF), can promote vessel dilation and sprouting. However additional stimuli like mechanical signals are also necessary for proper vascular morphogenesis. Owing to the evident interaction between biochemical and mechanical cues *in vivo*, several studies aimed at replicating such an interaction in specifically designed microsystems. This, of course, requires a tight control on the biochemical and biophysical characteristic of the cell microenvironment.

One strategy to control biochemical and mechanical stimulation may result from using devices, that isolate biochemical stimulus, for example through the use of hydrogel, and create controlled mechanical stimuli (such as interstitial flow). Several studies integrated biochemical and mechanical environment factors in 3D matrix using in vitro assays. For istance, the in vitro platform developed by Munn's group determined how fluid forces and chemical factors cooperated, to modulate sprouting from vessel analogous in vitro [20]. Vickerman et al. demonstrated the ability to generate gradients (non-reactive solute), surface shear, interstitial flow and they proved three different capillary morphogenesis assays [21]. One feature of the devices is that the environmental factors can be controlled independently allowing to isolate and define specific contributions of single factors as well as examine their possible interplays.

Mechanical stimuli, in the form of interstitial fluid flow are also known to influence the spatial distribution of cell-secreted biochemical proteins in the cell microenvironment. This mechanism, known as autologous chemotaxis, represents the ability of a cell to both produce and follow its own chemotactic gradient when interstitial flow is present. This aspect has a major role during growth and invasion of cancer cells [22-24]. In particular this mechanism is possible when the tumour cells secrete a chemokine for which it expresses the cognate chemokine receptor. Shields et al. showed that the breast cancer and melanoma tumour cells, expressing the chemokine receptor CCR7 and the ligand CCL21, exhibited an increased migration in the presence of interstitial flow *in vitro* [22]. Tumour cells located situated in the interstitial space were subjected to the interstitial flow pointing toward the lymphatic vessel. Cells secreting CCL21, formed a peri-cellular CCL21 concentration profile via molecular diffusion. This profile was symmetric with respect to the tumour cell in the absence of the flow; but skewed toward the flow when this was present [25] (Fig. 3).

The evaluation of the relative contribution of the convective vs. diffusive transport on mass transport, relies on the well know Peclet number *Pe*, that is the ratio vL/D; v, fluid velocity; L, characteristic length; D, diffusion coefficient , i.e. it represents the ratio of convective flow to diffusive transport. At low Peclet number (<1) the diffusive transport becomes the dominant mechanism. Conversely at high Peclet number (>1) convective transport is predominant. In a physiologically relevant context in close proximity to a cell (L ~ 20 μm), in which the interstitial flow rates in the 0.1-4.0 μm/s interval, and the diffusion coefficient of moprhogens (~10-100 kDa) fall within the 0.6-1.6 x 10-6 cm^2/s interval, the migration of proteins and macromolecules

is controlled by convection. Polacheck et al. observed that CCR7-dependent autologous chemotaxis was the mechanism that led to migration with the flow, whereas blocking of the receptor reversed the direction of migration (i.e. breast cancer cells migrated against the flow), and this upstream motion was mechanically mediated [23]. Cells are not the only source of biomolecules. In fact, the ECM constitutes an important reservoir of many morphogens and chemokines and the interstitial fluid flow mediates and modify the features of the molecular gradients that establish around cells. Experimental data showed that low interstitial flows (2–10 μm/s) acted in concert with fibrin-bound VEGF to enhance capillary morphogenesis [26].

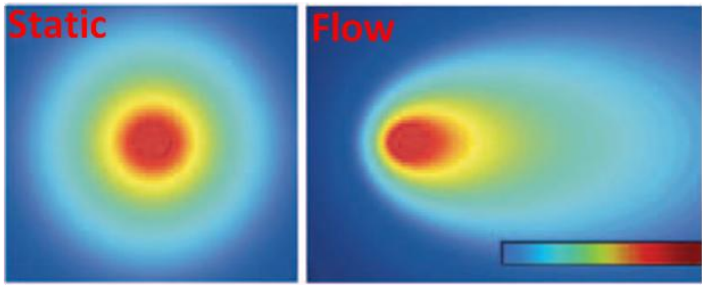

Figure 3. Autologous morphogen gradients under interstitial flow.

1.5 Microfluidics to Control Cell Microenvironment

Microfluidic platforms offer a powerful tool for replicating *in vitro* certain environments that are found *in vivo* and therefore they allow the systematic investigation of the phenomena regulating cell-extracellular microenvironment interactions for various biological applications (chemotaxis, angiogenesis etc.).

At the microscale the laws of physics remain the same as in macroscopic systems. However, the length scale of the network may depress or enhance certain forces or phenomena. For example due to the small length scale, fluid flow is laminar and mass transport through the liquid–liquid interface is possible only by diffusion, that mimics mass transport in tissues. The consequence of this phenomenon is a limited mixing that might take very long time [27] and promotes the occurrence of biomolecular gradients. Slow diffusive mixing can be a major limitation for some

applications requiring fast homogenization of flow but it can be corrected using efficient micromixing [28]. One dimensionless number that gives an indication of the flow regime is the Reynolds number, Re, and is defined

$$Re = \frac{\rho v L}{\mu}$$

where ρ is the density of fluid (1 g*cm^{-3} for water at 20°C),v is velocity of the fluid (typical 1-1000 μm*s^{-1}), L is typical length scale (1-1000 μm), μ is the fluid viscosity (1*10-2 g*cm^{-1}*s^{-1}). In microfluidic channels, the Reynolds number is usually below 100, this means the viscous forces are much larger then inertial ones. Therefore pressure driven incompressible flow is described by two equations, the Navier-Stokes equation:

$$\nabla p + \rho\,(v.\nabla)v = \mu\nabla^2\, v + f$$

and the equation for conservation of mss:

$$\nabla.v = 0$$

where v is the fluid velocity, p is the pressure, μ is the fluid viscosity, ρ is the fluid density and f is boding forces acting on the fluid. For designing microfluidic networks, the hypothesis of no slip boundaries is usually done. The exact solution of the equations depends on the cross sectional geometry of the microfluidic channel. However, the flows always follow a parabolic profile. The steady state velocity profile for a rectangular channel can be approximated by the parallel plate Poiseuille flow:

$$v_x(y) = \frac{\Delta p}{2L\mu}(h - y)y$$

The velocity in the x direction, v_x, is a function of the position along the channel height, y, and h is the channel height, ΔP is the pressure difference of the two ends of the channel, L is the length of the channel, and μ is the viscosity of the fluid. Flow profile can also be described conveniently using a fluidic resistance concept.

$$\Delta p = QR$$

The pressure drop, ΔP, is equal to the product of volumetric flow rate through a channel, Q, and fluidic resistance of the channel, R. For a rectangular channel, with the width much larger than the height, the fluidic resistance can be approximated as

$$R = \frac{12\mu L}{wh^3}$$

where w is the width of the channel, h is the height of the channel and L is the length of the channel.

The diffusion is the main mode of transport in the micronscale cell culture systems. Diffusion is the process by which particles move from higher concentration regions to lower concentration regions because of Brownian motion and their flux can be represented mathematically with Fick's first law of diffusion:

$$J = -D\frac{dC}{dx}$$

where J is the flux of particles, D is the diffusion coefficient, C is the concentration and x is the position. In one dimension, diffusion can be modelled by the equation:

$$d^2 = 2Dt$$

where d is the mean distance that a particle travels, D is the diffusion constant and t is the time. Diffusion becomes the dominant transport mechanism only at long time scales and/or short distances. The relation between convection and diffusion is given by Peclet number:

$$Pe = \frac{vL}{D}$$

where v is the velocity, L is the characteristic length, and D is the diffusion coefficient of the particle. For large Péclet numbers convection dominates, while slower velocities (or shorter lengths) cause diffusion to dominate. Pe can be used to estimate how long a channel has to be in respect to its width to achieve complete mixing for a certain flow velocity and diffusion constant. Peclet number can vary significantly in microfluidic system depending on the molecule of interest, channel size, and flow velocity. In general, the reduction of size, compared with

macroscale approach, has a direct influence on the time required for the diffusion of a molecule, which decreases as the square of the characteristic length.

The small dimension of microfluidic channels, results in a large surface area to volume (SAV) ratio, which means the superficial properties became important. Very large SAV ratios are advantageous in cell culture systems mainly because of the efficient mass transport of gases via diffusion to and from cells (assuming the microchannel is constructed of gas-permeable polymer). On the other hand, large SAV ratios can induce problems for micronscale cell cultures [29]. For example, surface adsorption becomes an important aspect during the design process. Proteins in culture medium are often internally hydrophobic and for this reason can be adsorbed to the certain surface. Many materials used in the fabrication of micro culture environments are also hydrophobic (i.e. Polydimethylsiloxane), for this reason the proteins are attracted to a nearby hydrophobic microchannel wall, causing the variation of the local media composition inside a microfluidic device [30]. Special measures need to be used to reduce their hydrophobicity, like oxidation of the surface via plasma treatment, binding of protein on the surface. Also, with the increase in surface area, evaporation happens at faster rates.

Surface tension also becomes non negligible at the micronscale. It can be used to drive the fluid flow. In fact, exploiting the tension effects a passive pumping method was developed to pump fluids inside microfluidic systems [31].

1.6 Microfluidic Devices as Gradient Generators

A wide variety of technologies, to carry out systematic studies of signal's effects on cellular behavior (migration, differentiation), were presented in the past decades. The conventional assays, including the under-agarose assay [32], Boyden chambers [33] (or transwell assays), the Dunn chamber [34] and the Zigmond chamber [35], have been widely used in the past in order to generate in vitro gradients of soluble molecules. However, these systems present intrinsic limitations due to large static volumes, lack of control on the gradient shape and steepness, and their length scale are not totally comparable with the native cellular microenvironment.

Microfluidic devices (μFCD) may help in solving the above mentioned issues since they in principle allow to gain a better control on the biochemical characteristic of the cell microenvironment.

A class of microfluidic devices use the property of laminar flow through diffusive mixing between two or more parallel laminar streams of different composition to generate molecular gradient. They are based on a premixing network connected to single microchannel where a complex profiles of concentration are generated [36-40]. An example of this approaches is the device of Jeon (fig. 4a), in which complex gradients of IL-8 are generated to study neutrophil chemotaxis [38]. This devices possess the advantage of establishing the gradient rapidly and its features can be modulated in time; the shape of the gradient depends on the flow rate and the time the streams are in contact. A drawback of this design is the "wash-out" effect of the fluid stream on the factors (autocrine or paracrine) secreted by the cells. Furthermore, the cells are exposed to both the chemical concentration gradient and shear stresses associated with fluid flow. This can create problems in assessing the individual contribution of gradient or shear in a specific cellular response. Finally, they are incapable to generate gradient profiles in a 3-D scaffold.

Concentration gradients in a microfluidic devices can be generated by exploiting flow resistive elements to eliminate convection around cells. This approach relies on the passive diffusion of biomolecules across membranes or hydrogels, that create a physical barrier to convective transport. In absence the fluid flow the shear stress exerted on the cells is negligible, secreted molecules persist in close proximity to the cell. Major drawback of these device is their inability to generate rapid and dynamic gradient profiles due to spontaneous diffusion. Abhyankar et al. fabricated a device in which two different membranes are used to isolate the gradient forming region from flow channels. The high resistance of membranes eliminates the fluid flow and allows the diffusion transport into the gradient region. The sink and the source region had a large volume to maintain the stability of gradient profile [41]. However, in devices with static reservoirs temporal stability of the gradient features cannot be achieved easily. Increasing the volume of reservoir might be a solution, however labile molecules may denature if maintained at high temperatures for long time frames. An alternative approach concerns the use a continuous flow (using an external pump or manual pipeting) that replenishes the source solute

concentration and eliminates the growing sink concentration. Diao et al. have developed a microfluidic linear chemical gradient generator for the study of bacterial chemotaxis. This device was fabricated in a membrane of nitrocellulose and consisted in three channels: two parallel channels separated by thin nitrocellulose wall from a central channel. The fluid flow within the side channels is driven by hydrostatic forces [42]. Cheng et al. proposed a device that derived the concept of the three channels design, but they used a different diffusion matrix (agarose) in order to eliminate the problems associated with the use of the membrane (poor permeability of proteins and long gradient establishing time)[43].

An alternative to the use of membranes and gels as physical barrier consist in employing microcapillaries that connect a cell containing chamber with the sink and the source channels. The interconnecting microcapillaries create a high fluidic resistance that restrict convective flow to allow diffusion [44]. However the use of microchannels does not eliminate convection but only minimize it.

The diffusion gradient-forming microfluidic devices, that have been described so far, are essentially limited to two-dimensional (2D) experimental setup. Cells culturing in a three-dimensional environment may mimic more closely the physiological environment, thus providing more reliable results. Several techniques have been employed to generate concentration gradients of soluble factors in 3D gels, to investigate cell response in tissues-like environments. Haessler et al. have used the three channels approach but they developed migration assays in a 3D microenvironment decoupling the flow control channels from the cell compartment (fig.4b) [45]. Saadi et al. have proposed a device termed ladder chamber to investigate cell migration across 2D surfaces and 3D gels within defined stable concentration gradient. The ladder chamber consists of two flow channel interconnected by an array of microchannels where the gradient of soluble factors is formed (fig.4c). The distinguishing feature of the ladder chamber is that it offers a parallelized high-throughput approach for both 2D and 3D environments and it possesses the advantage of not creating a physical barrier between the flowing fluid and the cell populated matrix. In fact in this case, molecular transport is ensured by diffusion within the gel eliminating the transport resistance which offers the agarose/membrane barriers [46]. However small perturbations or pressure oscillations cause the gel to detach from the walls of channels, thus impairing the control on the gradient features.

The above mentioned devices have been designed to generate linear concentration profile within 3D environment, several works also have proposed methods for obtaining nonlinear gradient profile. Shapes of the concentration profile depend on the geometry of gradient forming region. It is possible to obtain no-linear concentration profile using an asymmetric design for the gradient forming region [47, 48]. In addition the integration of on-chip microvalves and pneumatic actuation into microfluidic platforms allows to expose to gradients of dynamically switching shapes, direction and chemical species [49, 50].

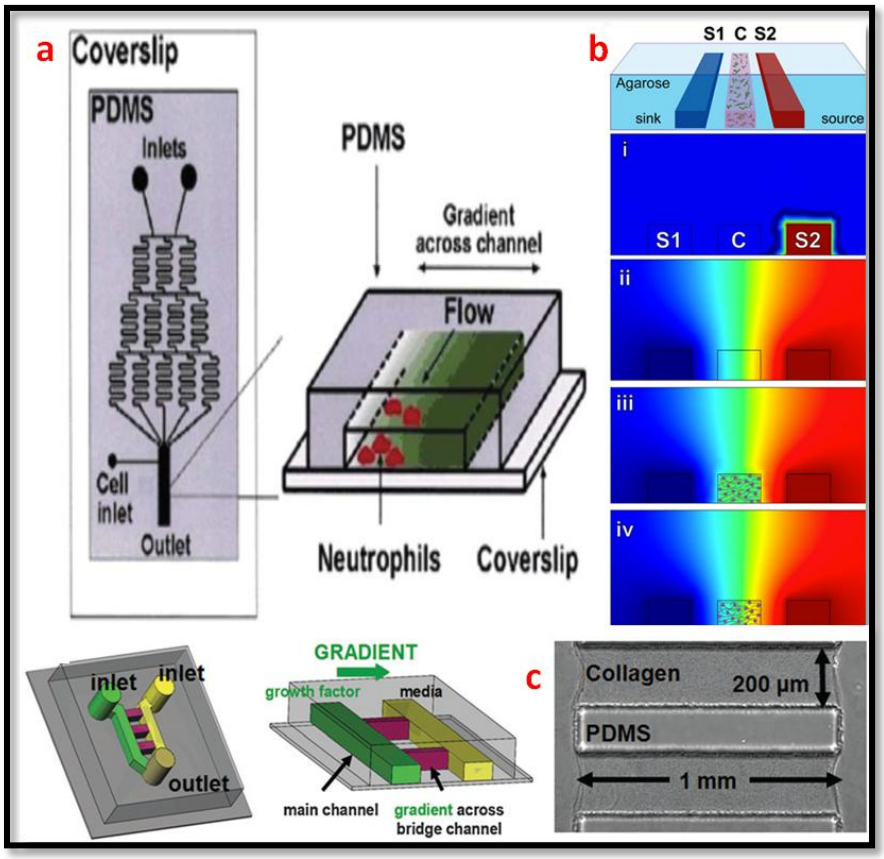

Figure 4 Microfluidic devices to generate biomolecular gradients. **a)** A convective flow based microfluidic device. **b)** The diffusion gradient-forming microfluidic device where the cells do no have direct contact with the flow. **c)** Ladder chamber.

1.7 Aims of Thesis

This thesis has focused the attention on development, design and optimization of devices to control the cell microenvironment in terms of soluble factors and shear forces. Physical and biochemical signals, or their combination, guide the cells in different biological processes. Therefore regulating the presentation of certain signals in three-dimensional space, and characterizing cellular response to signals is a very relevant topic in many disciplines. Therefore, the design and fabrication of versatile devices, along with the development of robust testing procedures is highly desirable. In fact, the deep understanding of specific cell responses to biochemical and/or biophysical stimuli can only be achieved if a tight and consistent control on cell microenvironment is possible.

This work is divided in two parts: in the first part the development and fabrication of a reliable and robust microfluidic device for the culture of mammalian cells in 3D environment, subjected to linear gradient of **biomolecular** signals is reported. In particular, the most frequent issues that could arise from non optimized designs, fabrication and testing procedure were addressed and technical solutions to these were proposed.

The second part of the work concerns the setup of an experimental procedure to investigate the role of mechanical forces, here as **interstitial fluid flow**, on tumor invasion and metastasis in 3D matrix.

1.8 References

[1] M.P. Lutolf and J.A. Hubbell, *Synthetic Biomaterials as Instructive Extracellular Microenvironments for Morphogenesis in Tissue Engineering*, Nat Biotechnol, **23**, 47-55, 2005.

[2] S. Sant, M. J. Hancock, J. P. Donnelly, D. Iyer and A. Khademhosseini, *Biomimetic Gradient Hydrogels for Tissue Engineering*, Can J Chem Eng, **88**, 899-911, 2010.

[3] O. Jeon, D. S. Alt, S. W. Linderman and E. Alsberg, *Biochemical and Physical Signal Gradients in Hydrogels to Control Stem Cell Behavior*, Adv Mater, **44**, 6366-6372, 2013.

[4] A. Khademhosseini, R. Langer, J. Borenstein, and J. P. Vacanti, *Microscale technologies for tissue engineering and biology*, Proc Natl Acad Sci USA, **103**, 2480–2487, 2006.

[5] S.F. Badylak, *The extracellular matrix as a scaffold for tissue reconstruction*, Sem Cell Devel Biol, **13**, 377–383, 2002.

[6] D. E. Discher, D. J. Mooney and P. W. Zandstra, *Growth Factors, Matrices, and Forces Combine and Control Stem Cells*, Science, **324**, 1673–1677, 2009.

[7] B. Moser and P. Loetscher, *Lymphocyte traffic control by chemokines*, Nat Immunol, **2**, 123–128, 2001.

[8] S.S. Verbridge, N.W. Choi, Y. Zheng, D.J. Brooks, A.D. Stroock and C. Fischbach, *Oxygen-Controlled Three-Dimensional Cultures to Analyze Tumor Angiogenesis*, Tissue Eng Part A, **16**, 2133–2141, 2010.

[9] J. Folkman, *Role of angiogenesis in tumor growth and metastasis*, Semin Oncol, **29**, 15–18, 2002.

[10] J.M. Rutkowski and M. A. Swartz, *A driving force for change: interstitial flow as a morphoregulator*, Trends Cell Biol, **17**, 44–50, 2007.

[11] S.R. Chary and R.K. Jain, *Direct measurement of interstitial convection and diffusion of albumin in normal and neoplastic tissues by fluorescence photobleaching*, Proc Natl Acad Sci USA, **86**, 5385–5389, 1989.

[12] H. Dafni, T. Israely, Z. M. Bhujwalla, L. E. Benjamin and M. Neeman, Cancer Res., *Overexpression of Vascular Endothelial Growth Factor 165 Drives Peritumor Interstitial Convection and Induces Lymphatic Drain*, **62**, 6731–6739, 2002.

[13] R.K. Jain, *Transport of molecules, particles, and cells in solid tumors*, Annu Rev Biomed Eng, **1**, 241–263, 1999.

[14] J.A. Pedersen, F. Boschetti and M.A. Swartz, *Effects of extracellular matrix architecture on velocity and shear stress profiles on cells within a 3-D collagen matrix*, J Biomech, **40**, 1484–1492, 2007.

[15] J.A. Pedersen, S. Lichter and M.A. Swartz, *Cells in 3D matrices under interstitial flow: Effects of extracellular matrix alignment on cell shear stress and drag forces*, J Biomech, **43**, 900–905, 2010.

[16] C.P. Ng and M.A. Swartz, *Fibroblast alignment under interstitial fluid flow using a novel 3-D tissue culture model*, Am J Physiol Heart Circ Physiol, **284**, 1771–1777, 2003.

[17] C.P. Ng, B. Hinz and M.A. Swartz, *Interstitial fluid flow induces myofibroblast differentiation and collagen alignment in vitro*, J Cell Sci, **118**, 4731–4739, 2005.

[18] S Wang, J.M. Tarbell, *Effect of Fluid Flow on Smooth Muscle Cells in a 3-Dimensional Collagen Gel Model*, Arterioscler Thromb Vasc Biol, **20**, 2220–2225, 2000.

[19] A. C. Shieh, H. A. Rozansky, B. Hinz and M. A. Swartz, *Tumor cell invasion is promoted by interstitial flow-induced matrix priming by stromal fibroblasts*, Cancer Res, **71**, 790-800, 2011.

[20] J. W. Song and L. L. Munn, *Fluid forces control endothelial sprouting*, Proc Natl Acad Sci USA, **108**, 15342–15347, 2011.

[21] V. Vickerman, J. Blundo, S. Chung and R. Kamm, *Design, fabrication and implementation of a novel multi-parameter control microfluidic platform for three-dimensional cell culture and real-time imaging*, Lab Chip, **8**, 1468–1477, 2008.

[22] J. D. Shields, M.E. Fleury, C. Yong, A.A. Tomei, G. J. Randolph, and M. A. Swartz, *Autologous chemotaxis as a mechanism of tumor cell homing to lymphatics via interstitial flow and autocrine CCR7 signaling*, Cancer Cell, **11**, 526–538, 2007.

[23] W. J. Polacheck, J. L. Charest and R. D. Kamm, *Interstitial flow influences direction of tumor cell migration through competing mechanisms*, Proc Natl Acad Sci USA, **108**, 11115–11120, 2011.

[24] U. Haessler, J. C. M. Teo, D. Foreta, P. Renaud and M.A. Swartz, *Migration dynamics of breast cancer cells in a tunable 3D interstitial flow chamber*, Integr Biol, **4**, 401–409, 2012.

[25] M.E. Fleury, K.C. Boardman, and M.A. Swartz, *Autologous morphogen gradients by subtle interstitial flow and matrix interactions*, Biophys J, **91**, 113–121, 2006.

[26] C. L. Helm, M. E. Fleury, A. H. Zisch, F. Boschetti and M. A. Swartz, *Synergy between interstitial flow and VEGF directs capillary morphogenesis in vitro through a gradient amplification mechanism*, Proc Natl Acad Sci USA, **102**, 15779–15784, 2005.

[27] H. A. Stone, A. D. Stroock and A. Ajdari, *Engineering flows in small devices: microfluidics toward a lab-on-a-chip*, Annu Rev Fluid Mech, **36**, 381–411, 2004.

[28] C.J. Campbell and B.A. Grzybowski, *Microfluidic mixers: from microfabricated to self-assembling devices*, Philos Trans A Math Phys Eng Sci, **15**, 1069-1086, 2004.

[29] G. M. Walker, H. C. Zeringue, and D. J. Beebe, *Microenvironment design considerations for cellular scale studies*, Lab Chip, **4**, 91-97, 2004.

[30] J.N. Lee, C. Park, and G. M. Whitesides, *Solvent compatibility of poly(dimethylsiloxane)-based microfluidic devices*, Anal Chem, **75**, 6544-6554, 2003.

[31] E. Berthier and D. J. Beebe, *Flow rate analysis of a surface tension driven passive micropump*, Lab Chip, **7**, 1475–1478, 2007.

[32] R.D. Nelson, P.G. Quie and R.L. Simmons, *Chemotaxis under agarose: a new and simple method for measuring chemotaxis and spontaneous migration of human polymorphonuclear leukocytes and monocytes*, J Immunol, **115**, 1650–1656, 1975.

[33] S. Boyden, *The chemotactic effect of mixtures of antibody and antigen on polymorphonuclear leukocytes, J Exp Med*, **115**, 453–466, 1962.

[34] D. Zicha, G. Dunn and A. Brown, *A new direct-viewing chemotaxis chamber*, J Cell Sci, **99**, 769–775, 1991.

[35] S.H. Zigmond, *Ability of polymorphonuclear leukocytes to orient in gradients of chemotactic factors*, J Cell Biol, **75**, 606–616, 1977.

[36] N.L. Jeon, S.K.W. Dertinger, D.T. Chiu and G.M. Whitesides, *Generation of solution and surface gradients using microfluidic systems*, Langmuir, **16**, 8311–8316, 2000.

[37] S.K.W. Dertinger, D.T. Chiu, N.L. Jeon and G.M. Whitesides, *Generation of gradients having complex shapes using microfluidic networks*, Anal Chem, **73**, 1240–1246, 2001.

[38] N.L. Jeon, H. Baskaran, S.K.W. Dertinger, G.M. Whitesides, L. Van De Water and M. Toner, *Neutrophil chemotaxis in linear and complex gradients of interleukin-8 formed in a microfabricated device*, Nat Biotechnol, **20**, 826–830, 2002.

[39] B.G. Chung, L.A. Flanagan, S.W. Rhee, P.H. Schwartz, A.P. Lee, E.S. Monuki and N.L. Jeon, *Human neural stem cell growth and differentiation in a gradient-generating microfluidic devic*e, Lab Chip, **5**, 401–406 , 2005.

[40] S.-J. Wang, W. Saadi, F. Lin, C.M.-C. Nguyen and N.L. Jeon, *Differential effects of EGF gradient profiles on MDA-MB-231 breast cancer cell chemotaxis*, Exp Cell Res, **300**, 180–189, 2004.

[41] V. V. Abhyankar, M. A. Lokuta, A. Huttenlocher and D. J. Beebe, *Characterization of a membrane-based gradient generator for use in cell-signaling studies*, Lab Chip, **6**, 389–393, 2006.

[42] J. Diao, L. Young, S. Kim, E. A. Fogarty, S. M. Heilman, P. Zhou, M. L. Shuler, M. Wu and M.P. DeLisa, *A three-channel microfluidic device for generating static linear gradients and its application to the quantitative analysis of bacterial chemotaxis*, Lab Chip, **6**, 381–388, 2006.

[43] S. Y. Cheng, S. Heilman, M. Wasserman, S. Archer, M. L. Shuler and M. Wu, *A hydrogel-based microfluidic device for the studies of directed cell migration*, Lab Chip, **7**, 763–769, 2007.

[44] H. Xu and S. C. Heilshorn, *Microfluidic Investigation of BDNF-Enhanced Neural Stem Cell Chemotaxis in CXCL12 Gradients*, Small, **9**, 585-595, 2013.

[45] U. Haessler, Y. Kalinin, M. A. Swartz and M. Wu, *An agarose-based microfluidic platform with a gradient buffer for 3D chemotaxis studies*, Biomed Microdevices, **11**, 827–835, 2009.

[46] W. Saadi, S. W. Rhee, F. Lin, B. Vahidi, B. G. Chung and N. L. Jeon, *Generation of Stable Concentration Gradients in 2D and 3D Environments using a microfluidic Ladder Chamber*, Biomed Microdevices, **9**, 627–635, 2007.

[47] V.V. Abhyankar, M.W. Toepke, C.L. Cortesio, M.A. Lokuta, A. Huttenlocher and D.J. Beebe, *A platform for assessing chemotactic migration within a spatiotemporally defined 3D microenvironment*, Lab Chip **8**, 1507–1515, 2008.

[48] B. Mosadegh, C. Huang, J. Park, H. Shin, B. Chung, S.-K. Hwang, K.-H. Lee, H. Kim, J. Brody and N. Jeon, *Generation of Stable Complex Gradients Across Two-Dimensional Surfaces and Three-Dimensional Gels*, *Langmuir*, **23**, 10910–10912,2007.

[49] D. Irimia, S. Y. Liu, W. G. Tharp, A. Samadani, M. Toner and M. C. Poznansky, *Microfluidic system for measuring neutrophil migratory responses to fast switches of chemical gradients*, Lab Chip, **6**, 191–198, 2006.

[50] T. M. Keenan, C. W. Frevert, A. Wu, V. Wong and A. Folch, *A new method for studying gradient-induced neutrophil desensitization based on an open microfluidic chamber*, Lab Chip, **10**, 116–122, 2010.

Chapter 2

Development and Fabrication of a Microfluidic Device for Generating Stable Concentration Gradient in 3D environment.

Introduction

Understanding the effects of gradients of soluble molecules is of paramount importance to unravel specialized cellular behaviours such as chemotaxis, angiogenesis, embryo development and tumour progression [1-3].

The practical implementation of gradients requires the use of specifically designed culturing devices and in the past decades several examples have been reported in the literature. Among these, Boyden chambers/ transwell assays [4], Dunn chambers [5] and Zigmond chamber [6], have been largely used. These systems, although instrumental in shaping our knowledge on the interplay between signal gradients and cells, present few drawbacks due to intrinsic limitations in controlling gradient features in time and space. Furthermore, they require the use of large volumes of conditioning media and are not readily scalable to native biological environments or other selected applications.

Rapid advancements in Microfluidics, provided new tools for a much more accurate control of the cellular microenvironment in terms of soluble molecules delivery. Microfluidic devices (μFds) proved to be very effective for the establishment of single or multiple gradients on 2D cell cultures. In particular a class of microfluidic devices use the property of laminar flow through diffusive mixing between two or more parallel laminar stream of different composition to generate molecular gradient. They are based on a premixing microchannels unit having different geometry combination and a cell culture area where a complex profiles of concentration are generated [7-11].

However, most of the mammalian cells are embedded in a 3D environment in vivo. This brings in a new level of complexity for the implementation of a 3D culture in microfluidics. Nevertheless, several elegant examples of 3D culture in μFd have been recently reported. For instance, Haessler et al. have developed an agarose-based 3D μFd in which the flow control channels is separated from the cell-containing matrix by an agarose gel wall [12]. In other μFd the cell populate matrix is in direct contact with the fluid flow in side channels [13,14]. These

examples, along with others, represent much more relevant models to study and allowed to shed light on the intricate mechanisms underlying cell responses to soluble signals that may occur in vivo.

Although these μFds may differ in terms of shape, dimensions and culturing conditions, they basically relies on the resistive effects of a cell laden biopolymeric gel on the soluble molecule of interest. This requires that the biopolymeric gel is homogeneous and stable within the μFd and that the conditioning media do not present fluctuation in composition. If these conditions are not met, the spatiotemporal features of the gradient might evolve unpredictably, thus impairing the control of the composition of the cellular microenvironment. For example, the presence of short cuts within the cell containing 3D matrix affects the spatial distribution of molecules, whereas matrix collapsing or local densifications may impair the diffusion mechanisms. Therefore, fluid-dynamic based problems or non controllable interactions between the device and the matrix can potentially cause the distribution of biomacromolecules to evolve towards states that can be very different from those originally intended.

The diffusion gradient-forming microfluidic device we developed presents an innovative design, in particular it eliminates the additive transport resistance of physical barrier (hydrogels or membranes) but on the other side the particular geometry of pillars deflects fluid streams in a way to promote the correct positioning of collagen.

We report a sequence of actions that should be undertaken in order to fabricate a reliable and robust microfluidic device for the culture of mammalian cells in 3D, subjected to linear gradient of biomolecular signals. In particular, we highlight most frequent issues that can arise from non optimized designs, fabrication and testing procedure and propose technical solutions to these issues. Finally, in order to prove the validity of the proposed method, we create linear gradients of bone morphogenetic protein 2 (BMP-2) within a 3D collagen gel and study the effects of gradient features on stem cell migration.

2.1 Materials and Methods

Design of Microfluidic Device

The microfluidc device consists in three parallel channels: a central channel, which is intended for containing the cell laden hydrogel and two identical channels juxtaposed to the hydrogel's lateral edges, in which culturing or conditioning media flow. The channels will be referred to as central channel and side channels throughout the text, respectively. The central channel, 1 mm in width and 300 μm in height, was designed in order to cultivate considerable number of cells, yet minimizing possible cell-cell contacts (sparse cell culture). The geometrical features of the side channels were chosen in order to minimize the volumes of the media employed during the experiments, yet sufficiently wide to minimize the shear stresses at the fluid-hydrogel interface, more specifically the side channels were 1 mm in width and in 300 μm height. Central and side channels are divided by an array of micro-pillars. Central and side channels are divided by an array of S-shaped micropillars (100 μm in width, 300 μm in height and 750 μm in length) (fig1).

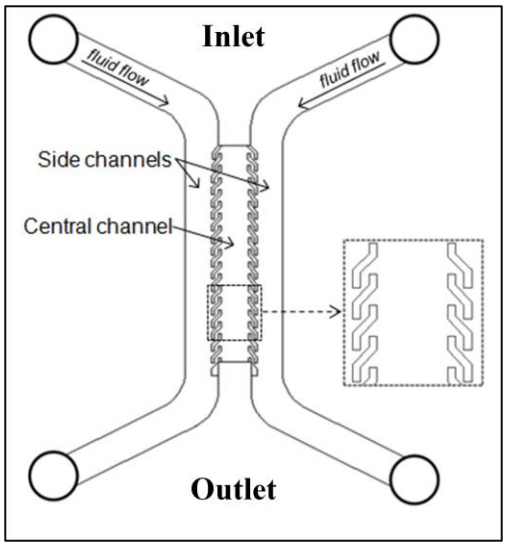

Figure 1. Schematic of the three channel μFd. Inset, magnification of the S-shaped pillars.

Computation Fluid Dynamics (CFD) and Transport Modeling

The fluid dynamics and the characteristics of the macromolecular transport in the hydrogel were computed through a multi-physics modeling software COMSOL (COMSOL Inc., Burlington, MA). The chamber was modeled in 2D model and the geometry was divided in 2 subdomains corresponding to the side channels and collagen gel region. The simulation was carried out by coupling *convection and diffusion* and the *incompressible Navier-Stokes* equations. For the molecular transport the diffusivity of a 10 kDa molecule with having diffusion coefficient of 2×10^{-6} cm^2/s in collagen gel was chosen [15]. The density of PBS (PHOSPHATE BUFFERED SALINE) and medium was 1000 kg m^{-3}, and the dynamic viscosity of PBS and medium was 10^{-3} kg m^{-1} s^{-1}. The concentration of the soluble molecules is always reported in terms of normalized values, thus varying from 0 to 1. The convective flux boundary condition at the outlet reported to purely convective mass transfer taking place at the outlet boundary and assumed that any mass flux due to diffusion across this boundary was zero. To solve the Navier–Stokes equation, the inlet fluid velocity for both streams was set to at the mean linear velocity which was obtained by dividing the volumetric flow rate (1µl/min) by the cross-sectional area of side channel, an outflow/pressure boundary condition was imposed at the outlet, and for all other surfaces, *no-slip* boundary conditions were used.

Fabrication and Assembly of Microfluidic Device

Blue print of the device was drafted in AutoCAD (Autodesk, CA). The microfluidic device was fabricated using a micromilling techniques and rapid prototyping. The master molds, in PMMA (Goodfellow, Huntingdon, England) were made using micromilling machine (Minitech CNC Mini-Mill).The device were produced by replica-molding of polydimethylsiloxane (PDMS) (Sylgard 184; Dow Corning, NY) on the master. The PDMS precursor and curing agent (10:1, w/w) were mixed, degassed under vacuum, and then cured against the PMMA master in an 70 °C oven for 1 h. Polymerized PDMS devices were peeled off the PMMA master, and the holes for the fluidic connectors were punched at the end of the side channels with a tissue biopsy puncher (1.5 mm diameter, Kai Industries). To close the fluidic micro-conduits the PDMS substrates were irreversibly bound to a 1 mm thick microscope glass slides via treatment with

plasma oxygen (Diener) for 1 min at 50 W. Once treated, the PDMS structure and glass coverslip were pressed together and then the sandwich was heated to 70 °C for 30 min to stabilize the bonding between the PDMS and glass. Afterwards, the μFd was sterilized by placing under UV light over night. In figure 2 a picture of microfluidic chamber with S-shape pillars, bound with cover glass, was reported.

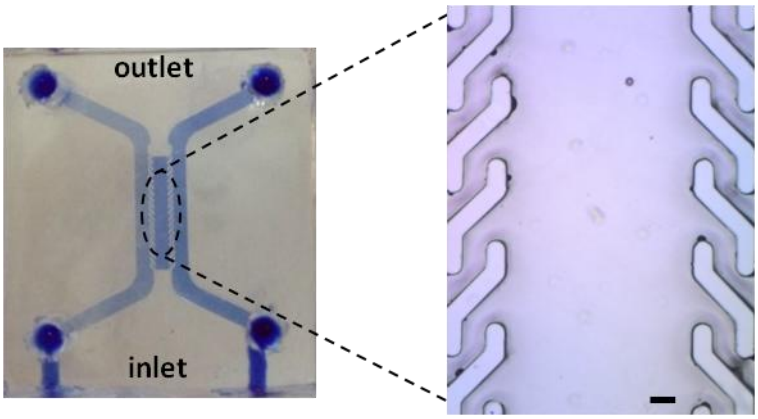

Figure 2. Picture of the microfluidic device with S-shape Pillars before gel loading. Scale bars: 100 μm.

3D Gel Preparation and Filling

Prior to filling with the biopolymeric gel, a collagen coating of the internal surfaces of the microfluidic device was performed. Briefly, a 50 μg/ml type I collagen solution (BD Biosciences) was loaded into the device. The device was then incubated at room temperature for one hour and then the proteic solution was aspirated and the channels were thoroughly washed with phosphate buffer solution (PBS).

After coating, collagen type I was added to a mixture containing 10x phosphate buffer solution (PBS), 1M NaOH, and tissue culture grade water to make a 3mg/ml prepolymer solution at 4°C. Then, the collagen solution was loaded into device from the one outlet as depicted in Figure 3a. The gas bubbles entrapped within the microfluidic device were removed by applying an overpressure [16]. Briefly, the two inlets and one outlet were closed with PDMS plugs and the collagen solution was forced through the device with a syringe pump (Harvard Apparatus, Standard Infuse/Withdraw Harvard 33 Twin) at 0.1 ml/min. Once the gas bubbles disappeared,

the excess collagen solution in the side channels was removed by suking it up with a micropipette from the inlets, as depicted in Figure 3b. The whole loading/unloading procedure was performed while the device was placed on a water/ice bath, to prevent collagen fibrillogenesis. Subsequently, the device was transferred for 15 min at 37°C in a humidified incubator to allow collagen fibrillogenesis. The channels were then filled loaded with PBS to prevent hydrogel dehydration and the device was placed back in the incubator for additional 15 min to complete the process of polymerization.

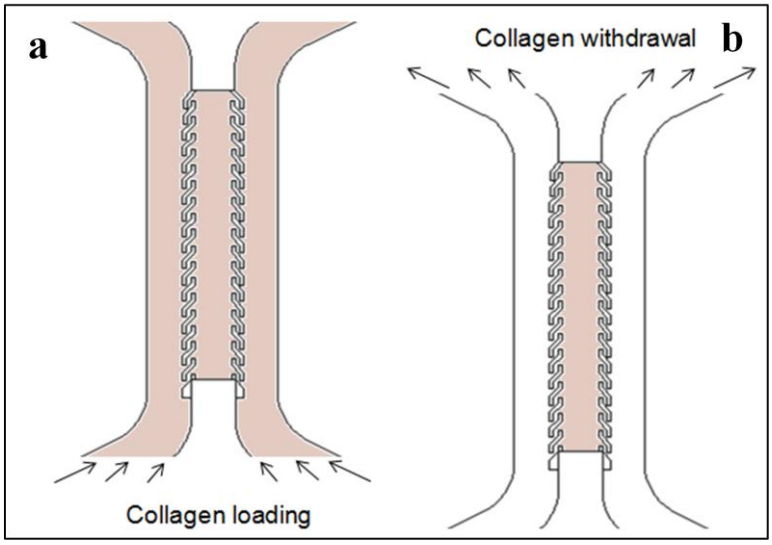

Figure 3. a) collagen solution loading process; **b)** collagen solution removal from the side channels.

Gradient Profile Characterization

To monitor gradient establishment and evolution a soluble fluorescent probe was used. In more details, after the loading and polymerization steps, a 10 µg/ml solution of dextran rhodamine (10 kDa, Molecular Probes) in PBS was injected with the syringe pump in one side channel (source), whereas pure PBS in the other side channel (sink). Flow rate was set at 1 µl/min for both solutions. The device was placed under a confocal laser scanning microscope (LSM510, Zeiss) and the fluorescence images were collected by exciting the channels with a HeNe laser (543 nm) and collecting the emission with a high pass filter (633 nm). Images were acquired every 30 min for 24 h. Time lapse videos were analyzed using ImageJ with which intensity profiles of

grayscale images were extracted. In particular, the profiles were obtained by averaging all the cross sections constituting the central channel.

Cell Culture and Chemotaxis Experiment

Human Mesenchymal Stem Cells (hMSCs) were purchased from Lonza and were expanded in alpha Modified Eagle's medium (αMEM, Bio-Wittaker) containing 10% (v/v) foetal bovine serum (FBS, HyClone), 100 U/ml penicillin, 0.1 mg/ml streptomycin and 2mM L-glutamine (Sigma). Cell cultures were kept in a humidified atmosphere at 37°C and 5% of CO_2 and the medium was replaced every 3 days. Cells were trypsinized by standard protocol and washed in PBS and resuspended in collagen solution (3 mg/ml) at the concentration 10^5 cells/ml. In order to maintain cell viability, the collagen-cell solution was injected in a μFd already containing a bubble-free collagen solution. In this case, the pre-existing liquid matrix allowed the collagen-gel solution to penetrate within the device without the formation of gas bubbles. Afterwards, the device was treated as previously described, with the only exception of using medium with 5% FBS in the side channels, in place of pure PBS we injected. The device was then placed in a humidified incubator for 12 h at 37°C.

Chemotactic gradients were generated by pumping with the syringe pump culture medium supplemented with BMP-2 (Peprotech, London, UK) in one side channel (source) and medium in the other channel (sink). To ensure proper gas exchange with the surrounding environment, gas permeable silicone tubing (GoodFellow) was used. Three different growth factor concentrations were employed, namely 1, 10 and 100 ng/ml, in order to obtain gradients with different features. Conversely, control experiments characterized by uniform distribution of BMP-2 were performed by injecting solutions containing the same factor concentration in both channels. Flow rates of the media were set at 1 μl/min.

Chemotaxis experiments were performed with an Olympus IX 50 optical inverted microscope equipped with a mini incubator on a motorized stage (PRIOR). The μFd and the tubing were placed in the mini incubator and images of the central channel were collected with a 4x magnification objective and a digital camera (CoolSnap Camera, Photometrics) thus obtaining 1.6 x 1.2 mm grayscale images. These were acquired every 10 min for 24 h. The images were

focused on five different section of the central channel. In each experiment 50-100 cells were focused

Data Analysis

The cell population within the central channel was divided into two separate areas: the grad+ and grad - area. The grad+ area was the one closest to the source channel while the grad- area was the farthest. The samples at uniform concentration were not divided into portion for the trajectories analysis. Cell trajectories were extracted from the time lapse videos analyzed with Metamorph (Molecular Devices). Drift speed of the cell population along the gradient (S_D) and chemotactic index (CI) were chosen as the representative parameters to quantify gradient effects on hMSC migration. S_D is estimated by plotting the average position of the cell population along the gradient direction against time. S_D is then evaluated by fitting the average position of the cell population with a straight line. CI is defined as the ratio of length of the cell trajectory with the magnitude of the head-to-tail vector of the trajectory. S_D values were considered to be significantly different if the corresponding 95% confidence intervals were non-overlapping. Kruskal-Wallis test was performed to assess significant differences among CI values. Calculations were performed with Matlab (The Matworks).

2.2 Results and Discussion

Numerical Simulation

In order to verify that the novel design was still effective in allowing the establishment of a concentration gradient within the cell containing matrix, numerical simulations firstly were performed. Generally, the generation and maintenance of a stable concentration gradient between the source and the sink depends on the diffusion coefficient of the diffusing molecule within the hydrogel as well as on the geometrical features of the device. The simulation was performed using the diffusion of 10 kDa dextrane molecule having a diffusion coefficient of 2×10^{-6} cm^2/s in collagen gel [15] for three different pillars' spacing: 450 μm , 650 μm, 900 μm. In case of 450 μm gap between consecutive pillars existed a stable gradient established after 6h (Fig. 4a).

Afterwards, the influence of pillar spacing on gradient features was assessed. In particular in the case of pillar spacing of 650 μm or 900 μm, the gradient was established in approximately in 5h or 4h respectively (Fig. 4b, Fig.4c). Gradient features, reported in terms of normalized values, for different pillar'spacing are summarized in Table 1. A trend increasing of gradient with increasing of pillar'spacing was observed. Both average concentration and slope are affected by pillar positioning.

The procedures reported in the following, concerning device fabrication and testing, refer to the geometry of Figure 4a. These, however, are of general validity that can be extended to the other designs.

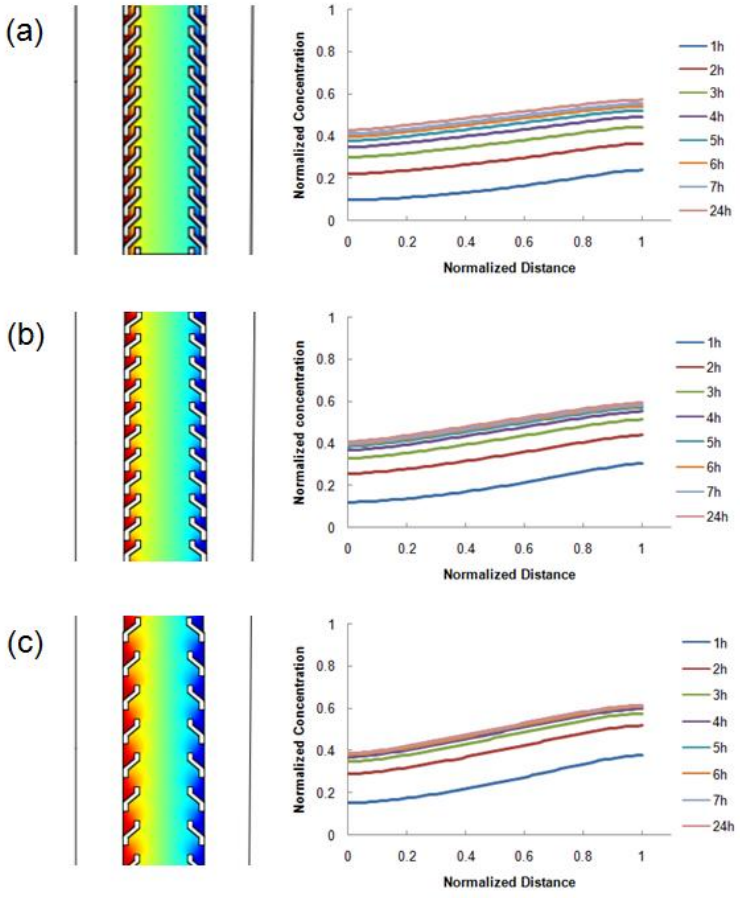

Figure 4. Time evolution of the concentration profile of 10 kDa dextrane molecule, having diffusion coefficient of 2×10^{-6} cm^2/s in collagen gel, as evaluated from the numerical simulation with COMSOL, for three different pillars' spacing: 450 μm (a); 650 μm (b); 900 μm (c).

TABLE I. Gradient, reported in terms of normalized values, for three different pillar'spacing.

Pillar'spacing	*450μm*	*650μm*	*900μm*
Gradient	0.16	0.2	0.25

Optimization of Gel-Wall Attachment

Microfluidic devices that allow cell culturing in 3D networks are usually designed in order to entrap the cell-laden hydrogel between arrays of microposts, while conditioning fluids or culturing media flow laterally [12-14]. Usually, the whole device is firstly filled with the matrix, in a liquid state, and subsequently a liquid is forced through the side channels thus allowing the biopolymer to polymerize only in a selected region of the device. However, if this procedure is not undertaken with care, a gel-wall detachment can occur. Detachments may cause fluids to penetrate within the gel compartment thus significantly altering the microenvironment in a non-controllable manner and the gel is not secured to the device and can wobble or float (fig.5).

To improve this, we changed the geometry of the pillars in order to increase the contact area, yet allowing macromolecules to diffuse within the hydrogel. Pillars were shaped in the form of a 'S', which physically locks the hydrogel since this penetrates within the pillars' coves. Furthermore, the peculiar S-shape enables a complete and effective removal of the hydrogel in excess (during the hydrogel loading/unloading phase) since the off-axis pillars' winglets deflect the fluid flow from penetrating inside the central channel thus damaging the hydrogel.

In order to increase the adhesion strength between the PDMS and the collagen gel, we performed a collagen precoating of the inner surfaces of the microfluidic network, prior to the hydrogel loading phase. This causes collagen molecules to firmly adsorb onto the PDMS surface, which constitute nucleation points for the collagen fibrillogenesis to occur. Indeed, we observed a strong interaction between the PDMS and the proteic gel with no evident formation of gaps in between.

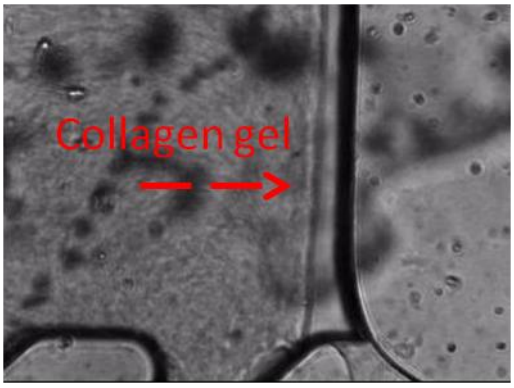

Figure 5. Gel-wall detachment due to lacking adhesion of the biopolymer to the elastomeric surface.

Gas Bubbles in the Gel Matrix

The presence of gas bubbles in the matrix occurs very frequently. This happens since cells need to be thoroughly homogenized within the gel and air bubble can be entrapped in the viscous biopolymeric matrix in the mixing process. Additionally, during the matrix loading process, bubbles may firmly adhere to the device's walls (fig. 6a) and once formed are impossible to remove. Although their dimension can be initially very small, (~100 μm), the bubbles invariably grew in time owing to the pressure gradients that establishes when a fluid is forced through the channels [17]. This causes the air bubbles to expand rapidly during the cell culture experiment (fig.7). Expansion forces are so high that cause matrix collapse and disturb the cell culture environment.

To address this problem, several reports have described methods by filling the complex microfluidic devices with aqueous solutions under vacuum [18,19]. These methods are simple and useful techniques to enable a bubble-free preparation. However, they are able to remove the instant appearance of bubbles during the microfluidic operation but they require additional vacuum systems. Additionally, vacuum can be harmful for cells. In general the trapped bubbles within a gas permeable polymer such as PDMS can disappear by gas diffusion through the elastomeric wall. However, this process is in general unpredictable since it depends on the thickness of PDMS, the dimension and the number of bubbles. Consequently it is necessary not only a more general method to eliminate the bubbles trapped in the microfluidic devices but also to predict the removal rate of gas bubbles in order to avoid the collagen gel fibrillation at room temperature.

In this work, the bubbles, both those within the gel and those attached to the wall, are removed by applying an overpressure. This method consisted in uniformly applying the pressure over the devices, in particular the collagen solution from one inlet is forced, while the other ports were kept closed with silicone plugs. Owing to the good gas permeability of the PDMS, bubbles under pressure permeate through the PDMS walls (fig. 6b) [16]. The procedure takes few minutes and cell viability is not affected by the pressure increase because the cell suspension is loaded into the central channel, containing the gel in a liquid state, after removing of bubbles.

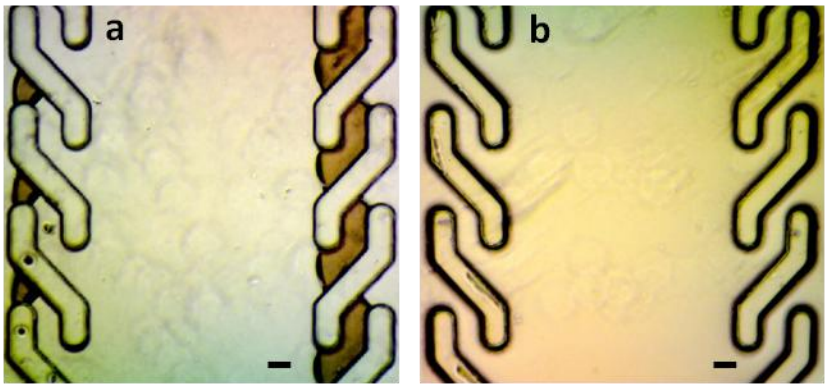

Figure 6. Bubbles removal. **a)** Air bubbles trapped within 3D collagen gel matrix. **b)** Air bubbles were successfully removed from the PDMS micro-pillars by applying an overpressure. Scale bars: 100 μm.

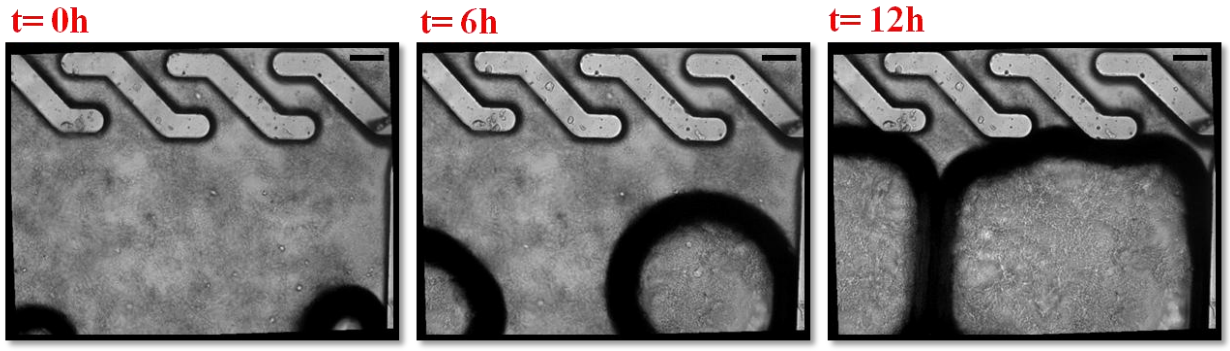

Figure 7. The experimental data plots of growth bubbles area within the collagen matrix during the cell culture experiment. Scale bars: 100 μm.

Gas Bubbles in the Side Channel

Unfortunately, biopolymeric matrix is not the only source of air bubble formation. Cell cultures require the use of gas saturated media that are necessary to maintain pH and oxygen concentration at physiologic values. When cultures are performed in microfluidics media are usually contained in tubes and sealed reservoirs. For long term experiments, gas may separate from the medium, thus creating bubbles. These, owing to the low flow rates (1 μl/min) reside in the side channels, near the cell containing matrix, for long times (fig. 8a). This causes the gel to dry out quickly, but most importantly alters the distribution of the soluble macromolecules.

To prove this a time-lapse experiment, was performed. In this experiment the diffusion of fluorescently labelled dextran through the collagen gel was monitored with confocal microscope. In Figure 8b the fluorescent intensity profile is reported when in the side channel, containing the dextran solution, the bubble is appeared after 10h. The presence of the bubble in the side channel alters the formation and maintenance of a stable gradient over time. Although the bubble does not appear until after 10 hours, its negative effects on the concentration profile can be seen starting even before this time. Apparently, when the bubble is in the tube prior to entering the side channel it impedes the flow of fresh solution. The dextran solution in the channel gradually discharges, while the bubble prevents any new fresh dextran from flowing in. For this reason, we observed a linear concentration profile with a slope that tends to zero. Approaching gas bubbles alter the fluorescent intensity profile promptly and significantly.

Therefore, gas bubbles must be separated from the fluid stream immediately before they could enter in the lateral channels. To this aim, we added two bubble traps in the form of a gas vent, one per each inlet. The trap consisted in a cylindrical hole (2.5 mm in diameter and 2.5 mm in height) punched in correspondence of the side channel ports. The hole was sealed with a silicone membrane through which a syringe needle was inserted. The connector above the needle was capped with a filter (0.22 mm pore size) to prevent bacterial contamination. Figure 9 shows the μFd in its final configuration.

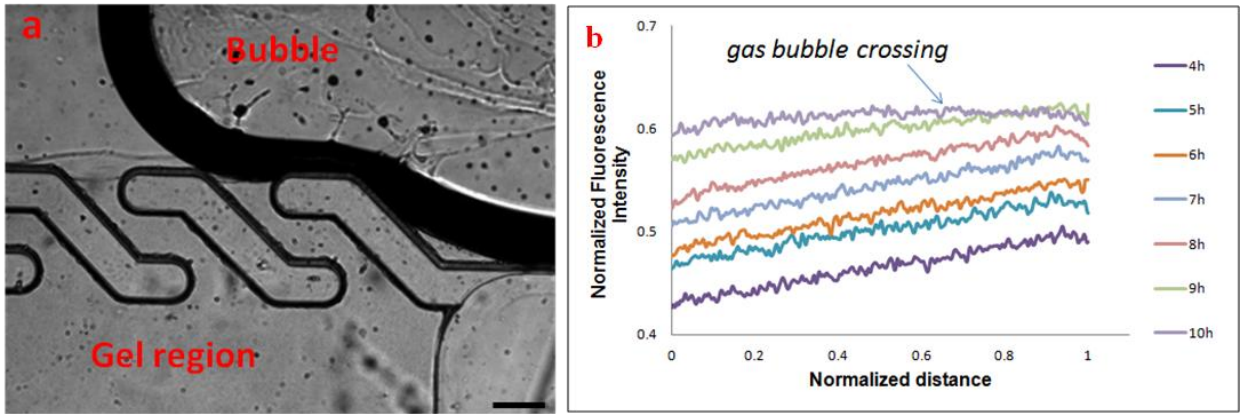

Figure 8. a) Bubble, near the cell containing matrix, occlude the microchannel and impede flow. **b)** Time evolution of fluorescence intensity profile affected by the presence of bubble in the side channel.

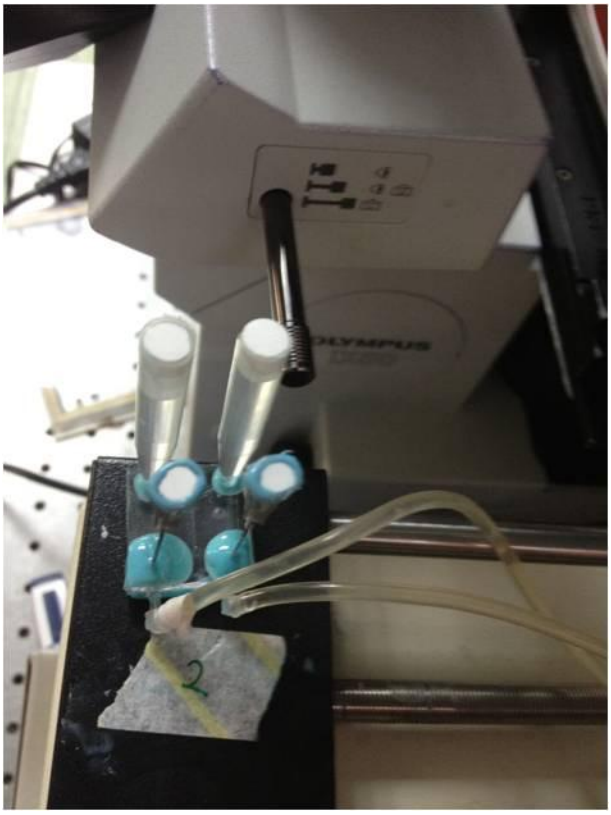

Figure 9. Top view of the final setup with the bubble trap in close proximity of the fluid inlets.

Gradient Characterization

To characterize the diffusion and the formation of concentration gradients across the gel region, rhodamine-dextran (MW 10 kDa) which is similar in size to BMP-2, was used. In particular, the spatio-temporal evolution of the diffusing molecule was evaluated as the variation of the fluorescence intensity, visualized through confocal microscopy. Rhodamine-dextran diffused between the source and sink channels across the gels, and the gradient developed in the central channel (fig.10).

In figure 11 the spatial and temporal concentration profile up to 10-hour period is reported. After 6h a linear gradient concentration was presented between the maximum concentration at the source channel and the minimum concentration at the sink channel and it remained stable during the whole experiments. Within this time frame, the spatio-temporal evolution of the molecular probe in the gel region was in close agreement with the theoretical results (fig.3a), that assumed a diffusion coefficient of $2*10^{-6}$ cm^2 s^1 for Rhodamine-dextran (10 kDa) in dilute solutions. The concentration value from Rhodamine-dextran calibration is higher than that of computation after 3 hours. This is due to accumulation of molecular probe into the gel during the diffusion; the computation did not take into account the portion of the dextran which binds with collagen.

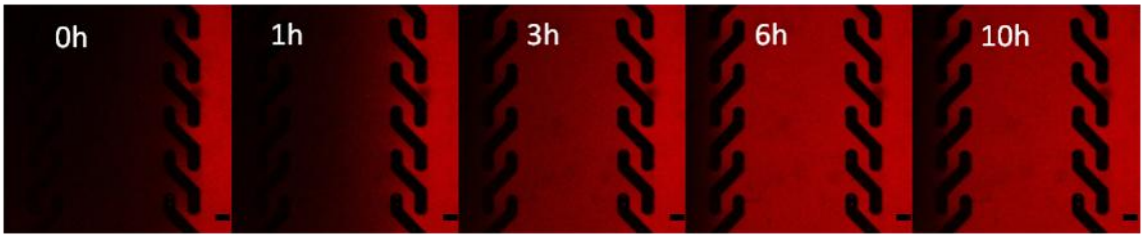

Figure 10. Temporal evolution of the diffusion of the fluorescent molecule in the central channel. Right and left inlets were loaded with Rhodamine-dextran (red) (MW 10 kDa) and PBS (black), respectively. Scale bars: 100 μm.

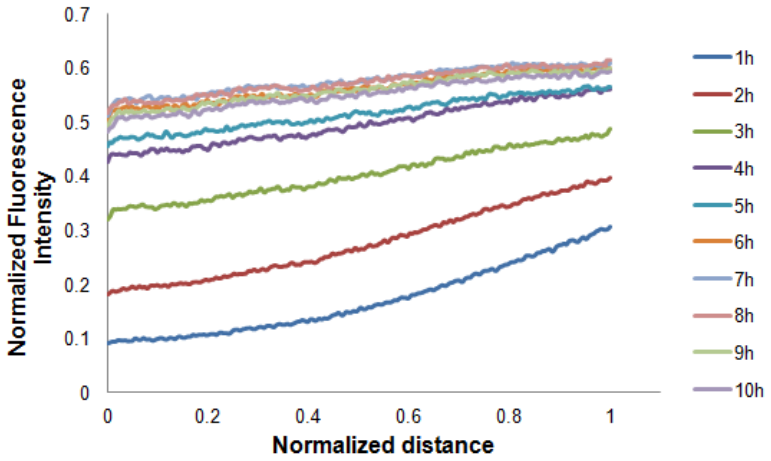

Figure 11. Plot of the fluorescence intensity profile across the gel region as a function of time. A linear steady state gradient was established after 6h.

hMSC Migration in Response to BMP-2 Gradients

Finally, to validate the device, we set up a chemotaxis experiment of hMSC subjected to linear gradients of BMP-2. The understanding of the effect of chemotactic gradients on cell motility requires a tight control of the gradient features over a large sample area and for sufficiently long time frames. In fact, cells and more specifically primary cells, display heterogeneous responses towards concentration gradients of soluble factors. Therefore, in order to draw definitive conclusions on cell behaviour during chemotaxis a statistically relevant number of cell must be tracked for long times. This means that the area for cell tracking must be large enough to contain at least 100 of isolated cells and that the gradient features are stable during the experiment and known a priori.

The growth factor BMP-2 has been widely studied as a potent signalling molecule that regulates bone regeneration in vivo and used in bone tissue engineering [20]. It also showed chemotactic effect in vitro on different cell types, among which osteoblastic cells [21], bone marrow stem cells [22] and microvascular endothelial cells [23]. However, the effect of specific presentation modes of the signal BMP-2, on cell migration in a 3D environment is not entirely known.

The microfluidic chamber we developed represents an ideal platform to address this issue. Therefore, hMSC, cultivated in the µFd, were subjected to linear concentration gradients of BMP-2. Cell migration was tracked for 24h while the cells were exposed to three different

gradient slopes namely, 0.16 ng/ml/mm, 1.6 ng/ml/mm, 16 ng/ml/mm. These values were calculated on the basis of the numerical simulations presented above for three different concentration of factor 1ng/ml, 10 ng/ml and 100 ng/ml. In steady state conditions, gradient slope value does not depend on the diffusion coefficient. However, in order to estimate also the time necessary for the gradient to establish, we extrapolated the diffusion coefficient of BMP-2 in collagen from the works of Vasaturo et al. [15], Vickerman et al. [24], and Ramanujan et al. [25] by assuming a molecular weight of 24kDa. In this case the time necessary for the gradient to establish is 8h (fig.12).

As reported in *material and methods* paragraph, for the cell tracking, the central channel was ideally divided in two halves, one closer to the BMP-2 source and the other closer to sink. In these regions, the average BMP-2 concentrations, evaluated through the numerical simulation, are reported in Table II. In the following we will refer to grad+ or grad- for the regions at higher or lower BMP-2 concentration respectively. This allowed us to obtain information on the synergistic effect of gradient slope and local average concentration of BMP-2.

Windrose plots of the hMSCs trajectories are reported in Figure 13. In presence of an uniform concentration of BMP-2, cell trajectories were isotropically distributed [Fig. 13(a-c)]. When BMP-2 gradient established, cell moved towards the zones with higher BMP-2 concentration. This was particularly evident in the 1.6 $ng \cdot ml^{-1} \cdot mm^{-1}$, 16 $ng \cdot ml^{-1} \cdot mm^{-1}$ cases [Fig. 13(e, f) and Fig. 13(h, i)].

To quantify the effects of gradient features on cell migration we evaluated the chemotactic index and the drift speed. The former provides an estimate on how effective cell motion is, i.e. CI close to 0 denotes a random motility, whereas CI ~1 implies that a cell describes a nearly straight path. This parameter, however, does not convey any directional meaning. Conversely, drift speed is the cell population's speed toward the chemotactic source. Interestingly we found that the increase in the uniform concentration of BMP-2 from 1 ng/ml to 10 or 100 ng/ml forced the cells to move more randomly, i.e. lower CI. A more effective cell migration is recovered as soon as signal gradient is established, irrespective of the relative position of cells with respect to the factor source [Fig. 14(a)]. Factor gradient had a profound effect on drift speed. In control experiments, i.e. uniform presentation of BMP-2, S_D was not significantly different from zero. In the case of signal gradients, a non-zero drift speed was observed. In particular, S_D increased with BMP-2 gradient slope in a dose dependent manner and the highest speed value was recorded in

the 16 ng·ml^{-1} ·mm^{-1} setup for the cells closest to the factor sink [Fig. 14(b)]. The speed was invariably higher for cells closer to the factor than for those closer to the sink, implying that not only BMP-2 gradient slope, but also local factor concentration exerts a major role in affecting cell migration.

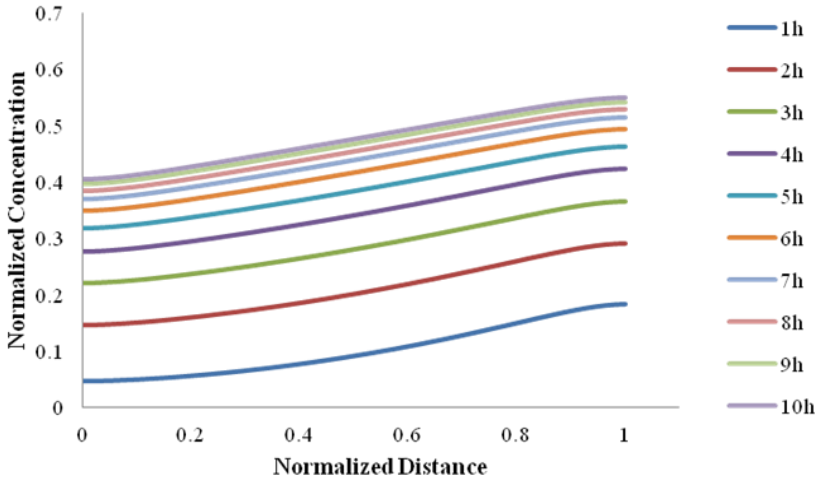

Figure 12. Concentration profiles evaluated from numerical simulations by assuming the diffusion coefficient of BMP-2 in collagen gel.

TABLE II. Average BMP-2 concentration [ng/ml] in the two microfluidic compartments

Gradient slope	*0.16 [ng/ml/mm]*	*1.6 [ng/ml/mm]*	*16 [ng/ml/mm]*
grad+	0.54	5.4	54
grad-	0.46	4.6	46

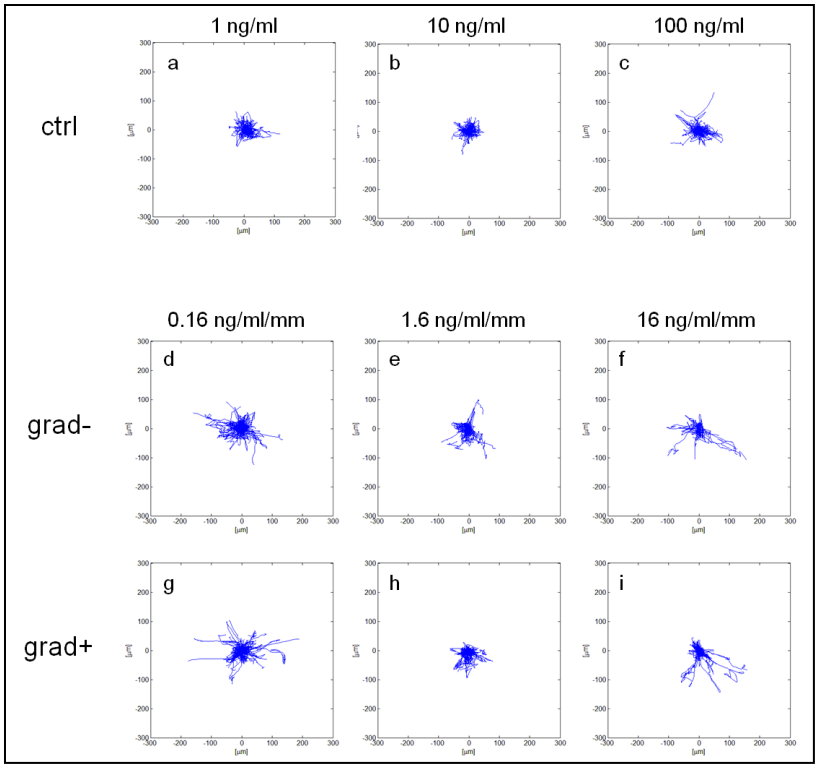

Figure 13. Windrose plots of hMSC trajectories recorded in the 24h cell tracking experiment. For the analysis of the results the central channel was divided into two areas: the grad+ and grad- area. The grad+ area is the one closest to the gradient of BMP2 while the grad- area is the farthest. The samples at uniform concentration(ctrl) were not divided into portion for the trajectories analysis. **a-c)** At uniform concentration of BMP-2, cells moved randomly and not polarized towards a certain direction **d-f)** Trajectories of cells, subjected to the gradient of 0.16 ng/ml·mm, 1.6 ng/ml·mm and 16 ng/ml·mm in the grad- area of the central channel. **g-i)** Trajectories of cells, subjected to the gradient of 0.16 ng/ml·mm, 1.6 ng/ml·mm and 16 ng/ml·mm in the grad+ area of the central channel. Each plot refers to a 300 x 300 μm area.

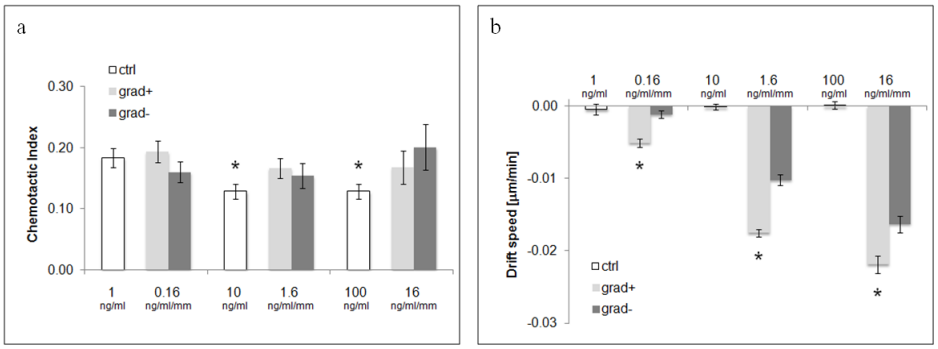

Figure 14. The representative parameters of cell migration for three different conditions of the gradients in both areas in which the central channel is ideally divided. **a)** Chemotactic Index values in case of uniform presentation of BMP-2 (white columns) or gradients (grey columns). * denotes significantly difference respect to the uniform 1 ng/ml case ($p<0.05$).**b)** Drift cellular speed values in case of uniform presentation of BMP-2 (white columns) or gradients (grey columns). In each group * denotes significantly difference respect to the grad- case ($p<0.05$). Error bars represent 95% confidence interval.

2.3 Conclusion

This study has concerned a method for the design, fabrication and testing of a microfluidic device for controlling cell microenvironment in three dimensional biopolimeric gels. The practical actions are focused to make the device as stable as possible thus allowing to achieve a high degree of consistency in the experimental procedure.

Three sources of potential inconsistency namely, hydrogel stability, local heterogeneities within the gel and gas-liquid separation of the culturing media were addressed. In fact, these problems may occur in large variety of experimental setups concerning cell cultures in microfluidic devices, irrespective from a specific design. Most importantly, these problems are those that most effectively have a detrimental impact in the control of the cell microenvironment. The proposed solutions are very easy to implement, cheap, do not alter cell viability and are sufficiently versatile to be applied to the majority of the microfluidic designs usually used for cell culturing experiments.

2.4 References

[1] L. Coultas, K. Chawengsaksophak and J. Rossant, *Endothelial cells and VEGF in vascular development*. Nature, **438**, 937-945, 2005.

[2] H. L. Ashe and J. Briscoe, *The interpretation of morphogen gradients*, Development, **133**, 385–394, 2006.

[3] E.T. Roussos, J.S. Condeelis and A. Patsialou, *Chemotaxis in cancer*, Nat Rev Cancer, **11**, 573–587, 2011.

[4] S. Boyden, *The chemotactic effect of mixtures of antibody and antigen on polymorphonuclear leukocytes, J Exp Med,* **115**, 453–466, 1962.

[5] D. Zicha, G. Dunn and A. Brown, *A new direct-viewing chemotaxis chamber*, J Cell Sci, **99**, 769–775 1991.

[6] S.H. Zigmond, *Ability of polymorphonuclear leukocytes to orient in gradients of chemotactic factors*, J Cell Biol, **75**, 606–616, 1977.

[7] N.L. Jeon, S.K.W. Dertinger, D.T. Chiu and G.M. Whitesides, *Generation of solution and surface gradients using microfluidic systems*, Langmuir, **16**, 8311–8316, 2000.

[8] S.K.W. Dertinger, D.T. Chiu, N.L. Jeon and G.M. Whitesides, *Generation of gradients having complex shapes using microfluidic networks*, Anal Chem, **73**, 1240–1246, 2001.

[9] N.L. Jeon, H. Baskaran, S.K.W. Dertinger, G.M. Whitesides, L. Van De Water and M. Toner, *Neutrophil chemotaxis in linear and complex gradients of interleukin-8 formed in a microfabricated device*, Nat Biotechnol, **20**, 826–830, 2002.

[10] B.G. Chung, L.A. Flanagan, S.W. Rhee, P.H. Schwartz, A.P. Lee, E.S. Monuki and N.L. Jeon, *Human neural stem cell growth and differentiation in a gradient-generating microfluidic devic*e, Lab Chip, **5**, 401–406 , 2005.

[11] S.-J. Wang, W. Saadi, F. Lin, C.M.-C. Nguyen and N.L. Jeon, *Differential effects of EGF gradient profiles on MDA-MB-231 breast cancer cell chemotaxis*, Exp Cell Res, **300**, 180–189, 2004.

[12] U. Haessler, Y. Kalinin, M. A. Swartz and M. Wu, *An agarose-based microfluidic platform with a gradient buffer for 3D chemotaxis studies*, Biomed Microdevices, **11**, 827–835, 2009.

[13] J. W. Song and L. L. Munn, *Fluid forces control endothelial sprouting*, Proc Natl Acad Sci USA, **108**, 15342–15347, 2011.

[14] W. Saadi, S. W. Rhee, F. Lin, B. Vahidi, B. G. Chung and N. L. Jeon, *Generation of Stable Concentration Gradients in 2D and 3D Environments using a microfluidic Ladder Chamber*, Biomed Microdevices, **9**, 627–635, 2007.

[15] A. Vasaturo, S. Caserta, I. Russo, V. Preziosi, C. Ciacci and S. Guido, *A Novel Chemotaxis Assay in 3-D Collagen Gels by Time-Lapse Microscopy*, Plos one, **12**, e52251, 2012.

[16] J.H. Kang, Y.C. Kim and J.K. Park, *Analysis of pressure-driven air bubble elimination in a microfluidic device*, *Lab Chip*, **8**, 176-178, 2008.

[17] L. Kim, Yi-C, Toh,J. Voldman and H. Yu, *A practical guide to microfluidic perfusion culture of adherent mammalian cells*, Lab Chip, **7**, 681–694 2007.

[18] I. Meyvantsson and D. J. Beebe, *Vacuum filling of microfluidic devices*, Chips & Tips (Lab on a Chip), 23 October 2006. http://www.rsc.org/Publishing/Journals/lc/vacuum_filling.asp;

[19] J. Monahan, A. A. Gewirth and R. G. Nuzzo, *A Method for Filling Complex Polymeric Microfluidic Devices and Arrays*, Anal Chem,**73**, 3193–3197, 2001.

[20] Y. Kimura, N. Miyazaki, N. Hayashi, S. Otsuru, K. Tamai, Y. Kaneda, and Y. Tabata, *Controlled Release of Bone Morphogenetic Protein-2 Enhances Recruitment of Osteogenic Progenitor Cells for De Novo Generation of Bone Tissue*, Tissue Engineering,Part A, **16**, 2010.

[21] K.N. Gonnerman , L.S. Brown and T.M. Chu, *Effects of growth factors on cell migration and alkaline phosphatase release*, Biomed Sci Instrum, **42**, 60-65, 2006.

[22] G. Pattappa, M. Peroglio, D. Sakai, J. Mochida, L.M. Benneker, M. Alini and S. Grad, *CCL5/RANTES is a key chemoattractant released by degenerative intervertebral discs in organ culture*, Eur Cell Mater, **27**,124-136, 2014.

[23] G. Li, Y. Cui, L. McILmurray, W. E. Allen and H. Wang, *rhBMP-2, rhVEGF165, rhPTN and thrombin-related peptide, TP508 induce chemotaxis of human osteoblasts and microvascular endo thelial cells*, J Orthop Res, **23**, 680-685, 2005.

[24] V. Vickerman, J. Blundo, S. Chung, and R. Kamm, *Design, fabrication and implementation of a novel multi-parameter control microfluidic platform for three-dimensional cell culture and real-time imaging*, Lab Chip, **8**, 1468-1477, 2008.

[25] S. Ramanujan, A. Pluen, T.D. McKee, E.B. Brown, Y. Boucher, and R.K. Jain, *Diffusion and convection in collagen gels: implications for transport in the tumor interstitium*, Biophys J, **3**, 1650-1660, 2002.

Chapter 3

Effects of interstitial flow on collective tumor cell invasion in a 3D model system

This work was carried out in the Laboratory of Lymphatic and Cancer Bioengineering (LLCB)of École polytechnique fédérale de Lausanne (EPFL)directed by Prof. Melody Swartz .

Introduction

Breast cancer is the most common cancer in women, representing the second most common cause of death in developed countries [1].

The factor responsible for the majority of cancer-related deaths is the development of metastasis to distant organs. Metastasis is the result of several sequential steps and represents a highly organized, non-random and organ-selective process [2]. Because of its primary impact on the disease's outcomes, it has been extensively studied. Many factors contributing to the success of the metastatic process were identified, spanning from the crosstalk of immune and tumour cells via secretion of IFNs (Interferons) [3] to stiffening of the ECM,[4] priming of the metastatic sites through exosome release [5] and genetic predisposition [6]. However, the cellular and molecular mechanisms that regulate the directional migration and invasion of the carcinogenic cells into the surrounding tissue, leading to metastasis in distant sites, have yet to be established. Mammary carcinomas originate from a polarized adult epithelium. After transition from a simple to multilayered organization, cells start to migrate collectively and invade the matrix.

Cell migration is a crucial process in cancer metastasis that involves a coordinated combination of cell adhesion and contractility, coupled with proteolytic remodelling of the extracellular matrix [7]. At the initial stages of cancer development and growth, collective type of migration is predominant in governing tumour invasion. During collective cell migration, cells move in coordinated groups and maintain cell–cell adhesion. The process is initiated by a group of leading cells, genetically different from the tumour core cells [8], and its evolution is promoted by the presence of a collagen I enriched matrix [9].

Metastasis of breast cancer occurs prevalently through the lymphatic system and the invasion of the sentinel lymph node, which while non-life-threatening itself, is a signal of bad prognosis [10-

13]. Therefore, the process of tumour lymphangiogenesis has been extensively studied, associating it to the consequent tumour cell intravasation into newly formed lymphatic vessel. Interestingly, intratumoral lymphatics have been correlated with increased invasion, metastasis and bad prognosis in different kind of carcinomas [14-16]. However, it has been shown that intratumoral lymphatics are often hyperplastic and non-functional, thus suggesting that lymphangiogenesis in cancer does not only impact tumour metastasis as a mere transport route, but potentially affects tumour cell migration through the modification of the local microenvironment.

Interstitial flow resulting from plasma leaking out from the blood capillaries and being drained by lymphatics, is highly upregulated in tumors, due to faulty blood vessels and to high interstitial pressure. Several groups have previously shown that interstitial flow influences tumour cell migration towards lymphatic vessel [17,18]. Issa et al. have used a transwell assay, where tumour cells and lymphatic endothelial cells (LECs) are cultured in separate but contiguous collagen gels, and they have shown that tumour cells secreting VEGF-C and expressing CCR7 can promote migration towards LECs. Once tumour cells reach the lymphatics, they must enter the vessel and then travel downstream to the lymphnodes [19]. Such studies focused on single cell migration. However, it is not clear whether interstitial flow influences collective invasion of the extracellular matrix. Furthermore, the effects of fluid flow on the lymphatic microenvironment it are not known.

Depending on the type of tumour cells, interstitial flow could influence cell migration in a variety of ways. Autologous chemotaxis [20] could be a valid mechanism in the context of collective migration. However, the tight contact between cells could alter the extracellular distribution of the chemotactic agent. Moreover, interstitial fluid could cause an increase in nutrient and oxygen transport in the tumour environment, provoking a decrease in the hypoxia levels. Hypoxia has been shown to have a dramatic impact on cancer development, inducing angiogenesis, matrix remodelling and stiffening [21,22]. One of the reasons behind the lack of knowledge about the effect of interstitial flow on tumour collective migration is the absence of experimental models. *In vivo*, the modulation of fluid flow rates is still a challenge. Furthermore, the *in vitro* systems that recapitulate physiological flows are designed for single cell movement analyses.

One of the *in vitro* systems that recapitulates more closely tumour development is the tumour

spheroid model [23]. It consists of the formation of 3D tumour organoids of 300 -800 μm in diameter through the cultivation of tumour cells on non-adhesive substrates. Carcinogenic cells start aggregating and with the help of medium additives as methylcellulose or matrigel, they form cellular spheroids [24, 25]. Such structures resemble the primary tumour *in vivo*, presenting a central necrotic core, a hypoxic ring and a highly proliferative outer layer [26]. Because of these features, they have been extensively used as model for anticancer drug screening [27].
Here tumor 3D spheroids with the application of interstitial flow in a radial flow chamber, as previously described, are combined [28]. Tumour spheroids recapitulate better the characteristics of carcinomas with respect to 2D cultures, and allow observation and quantification of collective migration, tumor-matrix interactions and tumour-stroma interactions [29-31]. A novel, integrated 3D model of murine breast cancer spheroids, with tunable interstitial flow is presented. The interstitial flow has reduced the sprouting of the murine 4T-1 cells.

3.1 Materials and Methods

Cell Culture

Mouse mammary carcinoma cell line 4T1 was maintained in DMEM with 10% FBS (all from Gibco, Invitrogen Corp., Carlsbad, USA) until 70–80% confluence. All cultures were kept in a humidified atmosphere at 37°C and 5% of CO_2; the medium was replaced every 3 days.

3D Spheroid Formation

Tumour spheroids were prepared as described previously [29]. Briefly, tumour cells were grown on plastic, trypsinized, counted and stained with cell tracker green if needed. Cells were then resuspended in DMEM medium with 10% foetal calf serum and 12 mg/mL of methylcellulose (Sigma-Aldrich, St. Louis, MO) and seeded into non-adhesive, U-shaped, 96- well plates for suspension culture (Cellstar®, Grainer Bio One, Kremsmuenster, Austria) at a concentration of 1000 cells per well. Compact spheroids were harvested after 3 days, washed and kept on ice until further use.

Radial flow chamber assembly

The protocol for the preparation of the radial flow chambers was adapted from the procedure described by Ng and collaborators [28]. The system consists in two petri dishes kept 1 mm apart by a porous polyethylene ring, between which a gel containing the cell spheroid is sandwiched.
The polyethylene rings were treated with sulfuric acid and abundantly washed with sterile water to render them hydrophilic. According to this procedure, the collagen gel adheres to the ring and does not contract in response to the cell tensile stress on the matrix.
Each ring was glued to the bottom of a 60mm petri dish with silicon glue (Dow corning) and allow to polymerize. Meanwhile, a 4 mm hole was drilled on the center of a 35mm petri dish, which was then glued on top of the ring, sandwiching it between the two plates. After the complete polymerization of the silicon glue, a 2.5 cm long piece of Tygon tubing (1.6mm i.d., 4.8 mm o.d.) was inserted in the central hole of the 35mm dish, to serve as fluidic inlet, and kept in place by a thin silicon glue layer (Fig.1).
The constructs were sterilized under UV light and were ready to be used for the experiment.

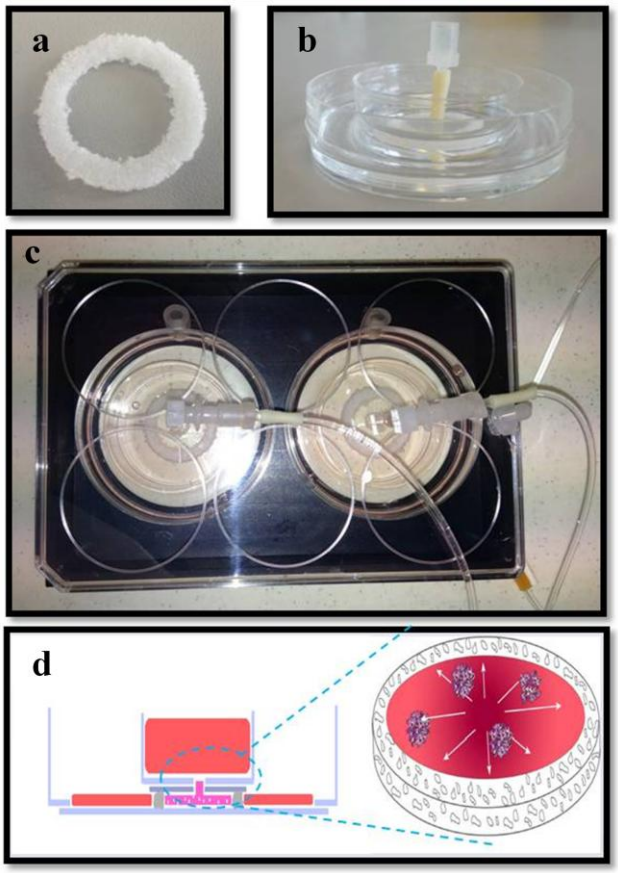

Figure 1. a) Picture of the porous polyethylene ring used for the chamber assembly **b)** Picture of a radial flow chamber before gel loading and **c)** top view of the final setup. **d)** Schematics of the spheroids in the radial flow chamber.

Estimation of the flow field in the flow chamber

The volumetric flow rates necessary to have the desired average flow velocities in the flow chamber were calculated analytically, considering the radial geometry, as follows:

$$v_r = \frac{Q}{2\pi r h}$$

$$\bar{v} = \frac{\int_{r_i}^{r_0} v\, dr}{\int_{r_i}^{r_0} dr} = \frac{\left[\frac{Q}{2\pi h}\ln r\right]_{r_i}^{r_0}}{(r_0 - r_i)} = \frac{Q}{2\pi h\,(r_0 - r_i)}\ln\frac{r_0}{r_i}$$

Where Q is the volumetric flow rate at the chamber inlet; r is the distance from the center; h is

the chamber height; is the average velocity in the flow chamber; r_i and r_0 are respectively the internal and outer radius between which the average velocity is calculated.

The complete flow pattern in the chamber where estimated computationally using Comsol Multiphysics. The chamber was modeled with a 2D radial axial symmetric geometry, and a triangular mesh composed of 6080 triangular elements. Interstitial flow was modeled with the Darcy equation:

$$\nabla p = -\frac{\mu}{ck} v$$

Where p is the pressure, v is the fluid velocity; μ is the fluid viscosity; k is permeability of the media, which was assumed to be 1e-6 cm^2, as derived previously by Ng et al. [32]. The Reynold's number was estimated to be between 10^{-5} and 10^{-6} for this system, validating the use of Darcy's law in modeling interstitial flow through the matrix.

A constant volumetric flow rate was imposed at the central inlet (r=0-2mm on the upper surface), while a constant pressure (P=0 Pa) was set at the outlet (r=8 on the lateral surface).

Spheroid sprouting experiment and quantification

96 tumor spheroids were suspended in 1500 µL of a 1.5 mg/ml collagen I (Rat tail collagen I, BD Bioscience) matrix with the addition of 5% Matrigel (BD bioscience). The gel solution containing the cell spheroids suspension was added in the flow chamber from the upper port (~300 µL per chamber, ~10-15 spheroids per chamber) and the gel was allowed to polymerize at 37°C for one hour.

Subsequently, two chambers were placed in a dedicated holder and sealed with a lid, which includes the ports for the interstitial flow tubes and for the gas supply. For the flow condition, a peristaltic pump (Ismatec Reglo Digital, IDEX, Glattburgg, Switzerland) was used to provide the desired flow rate. The tubes were connected to the inlets and the whole setup was transferred under the microscopes (Cell-IQ, CM-Technology, Tampere, Finland and Zeiss Axiovert 200M, Carl Zeiss, Germany), kept at 37°C and 5% CO_2. The flow was then started, setting inlet

volumetric flow rates of 0.0017 and 0.017 mL/min to obtain average flow velocities in the chambers of 1 and 10 µm/s, respectively. Images of the spheroids were acquired every 20 minutes for 12 hours. The images were post-processed with ImageJ, using differential operators to extract the borders of the spheroids and quantify their area at each time point (Fig, 2).

The volume was calculated using the formula: $V = \frac{2A}{3}\sqrt{\frac{A}{\pi}}$ where V is the spheroid volume and A is the measured area, assuming a spherical shape of the spheroid.

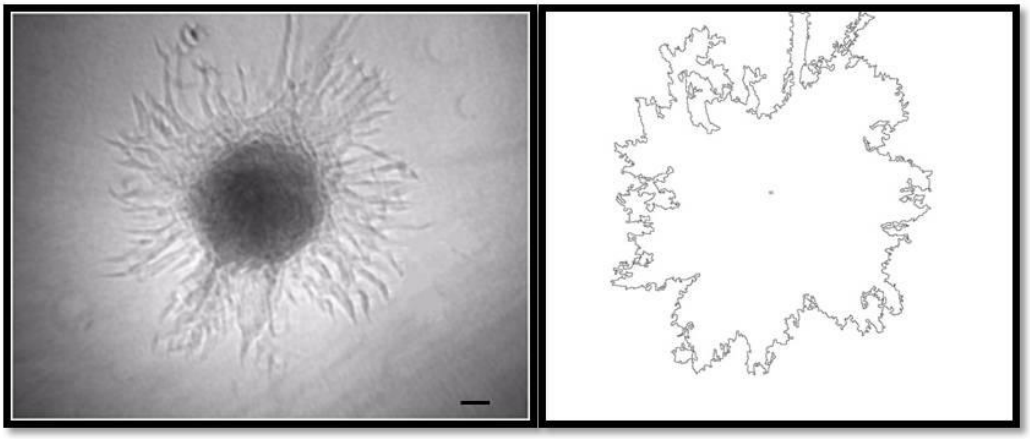

Figure 2. Spheroids were monitored over 12 hours, collecting images every 20 minutes. The left panel shows a picture of a 4T-1 spheroid after 12 hours in a collagen gel in static condition. The right panel shows the spheroid borders, which were extracted automatically using imageJ and used to quantify the spheroid area. Scale bar: 70 µm.

3.2 Results

Computational estimation of the interstitial flow field in the matrix

To predict the velocity profile in the flow chamber, a CFD model of the flow chamber was built. Because of the geometry of the chamber, we used a 2D axial symmetric model (Fig.3).

The results are in agreement with the analytical calculations of the average flow velocity in the chamber described in the *Material and Methods* paragraph. Imposing a defined inlet volumetric flow rate, the same average flow velocity in the chamber with the two distinct methods was obtained. Flow velocity profile obtained with a flow rate of 0.0017 mL/min at the inlet is reported in figure 3. In this case, a gradient of flow velocity is created in the gel that decreases with the distance from the centre, ranging from 1.8 to 0.5 µm/s. Setting an inlet velocity of 0.017

mL/min shifts the gradient of one order of magnitude. In both cases, the gradient small enough to be ignored in terms of the effect on the spheroids was considered. Consequently, for our measurement all the spheroids in the chamber were considered, excluding only those in proximity of the flow inlet region or at the external border.

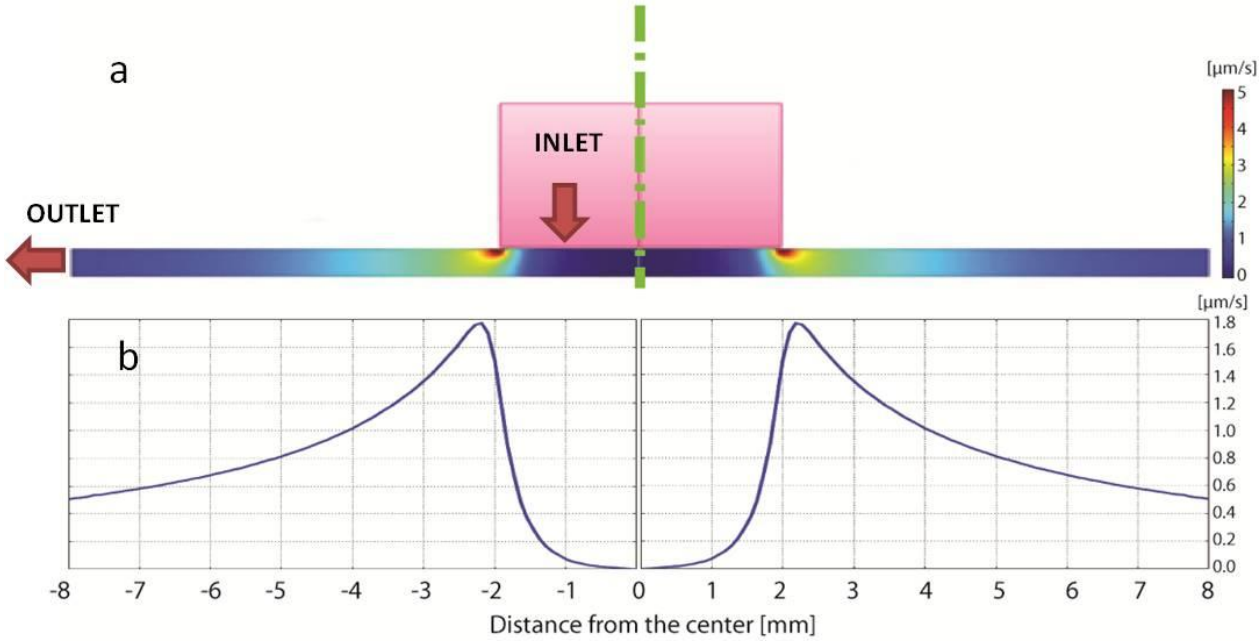

Figure 3. a) CFD computation of the velocity field in the radial flow chamber, given an inlet flow rate of 1.7x10-3 mL/min. **b)** Plot of the interstitial flow velocity in function of the distance from the center of the flow chamber, in the middle of the matrix thickness (0.5 mm from the bottom). In this condition, the average interstitial flow rate throughout the ECM is estimated to be 1 µm/s.

Interstitial flow decreases 4T-1 cell sprouting

To observe and quantify the effect of interstitial flow on the tumour spheroid growth and sprouting, the radial flow chamber system was adapted to allow the observation of tumour spheroids and multicellular spheroids in live microscopy. A plate capable of hosting 2 chambers was designed. In this way, using two microscopes, it was possible analyze 4 different conditions (or 2 conditions in duplicates) in the same experiment (Fig.1). Using the highly metastatic breast cancer cell line 4T-1 was developed.

The effect of interstitial flow on the collective cell migration of the murine breast cancer cell line 4T-1 was examined. The interstitial flow caused a marked decrease in spheroid sprouting

(Figure 4a and b). This effect appeared to be proportional to the interstitial flow rate.

To verify the presence of any preferential directionality of the observed sprouting reduction (i.e., cells stop sprouting only on one side of the spheroid), the centre of mass shift during the 12h of the experiment was measured (fig.5). In this case, directional bias was not detected.

4T-1 cells are not reported to express CCR7 or CCL19 that are implicated in the mechanism of autologous chemotaxis [33]. Nevertheless, they express other chemokines, as RANTES (CCL5), MCP-1 (CCL2) and MIP-1a (CCL3)[34]. Moreover, it has been reported not only that 4T-1 cells express CCR4, receptor for the ligands mentioned above, but also its expression is necessary for the 4T-1 cell to metastasize [35]. For this reasons a possible flow-dependent increase in spheroid sprouting in the flow direction due to the autologous chemotaxis mechanism would have expected.

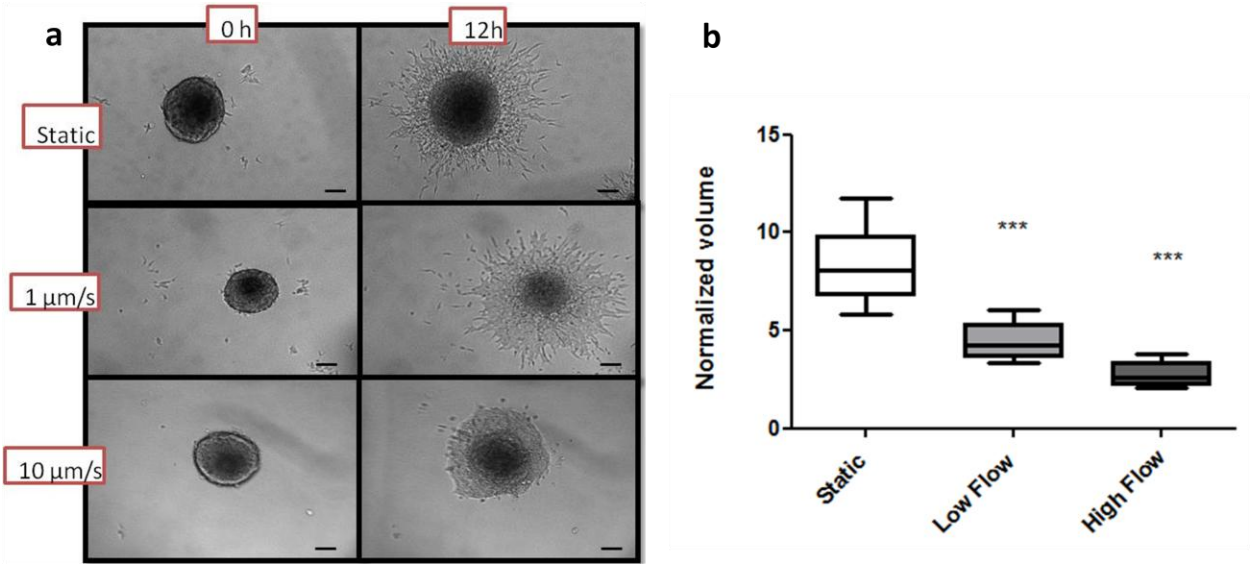

Figure 4. a) Pictures of the 4T-1 tumor spheroids embedded in the collagen I matrix in the radial flow chamber, in static and flow conditions, at 0 and 12 hours after they had been suspended in the ECM. **b)** Quantification of the spheroids volume after 12 hours from the beginning of the experiment. For each spheroid, the calculated value was normalized for the volume measured at time zero. ***: $P<0.0001$, calculated using the unpaired student t-test. Scale bars: 70 µm.

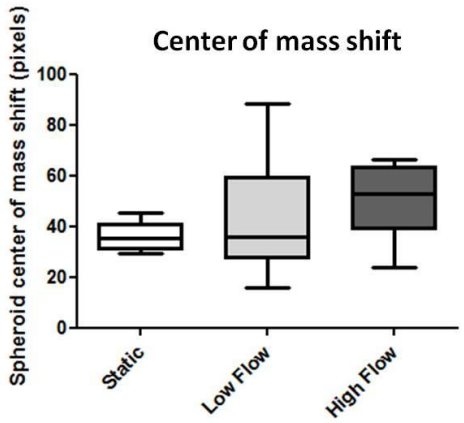

Figure 5. Plot of the center of mass shift of the 4T-1 spheroids in static and flow condition after 12h of culture in a collagen I gel in the radial flow chamber.

The fact that an opposite effect was observed suggests that there could be another mechanism playing a predominant role. It is tempting to speculate that such mechanism could be related to a flow-dependent downregulation of the CCR4 receptor or any of its ligands, although there is no similar hint in the literature. One of the most important factors in promoting metastasis in the 4T-1 cancer model is hypoxia [36, 37]. Indeed, hypoxic cells produce proteins as HIF-1α and LOX that have been reported to affect increase metastasis acting directly on cells or indirectly, remodeling the matrix by collagen crosslinking [38].

To investigate whether the decrease in spheroid sprouting, observed here, can be linked to the reducing hypoxia-dependent protein expression, we repeated the same experiment blocking the HIF-1α protein with sodium nitroprusside (SNP) which spontaneously releases nitric oxide (NO) donors that suppresses the activation of HIF-1α protein [39]. In particular we observed that the addition of SNP, in the collagen and in the medium at a concentration of 200 μM, reduced the tumour sprouting in absence of flow but had no effect in flow condition (Figure 6). In facts in this last case the interstitial flow has the potential of reduced hypoxia-dependent protein expression and the consequent tumour sprouting.

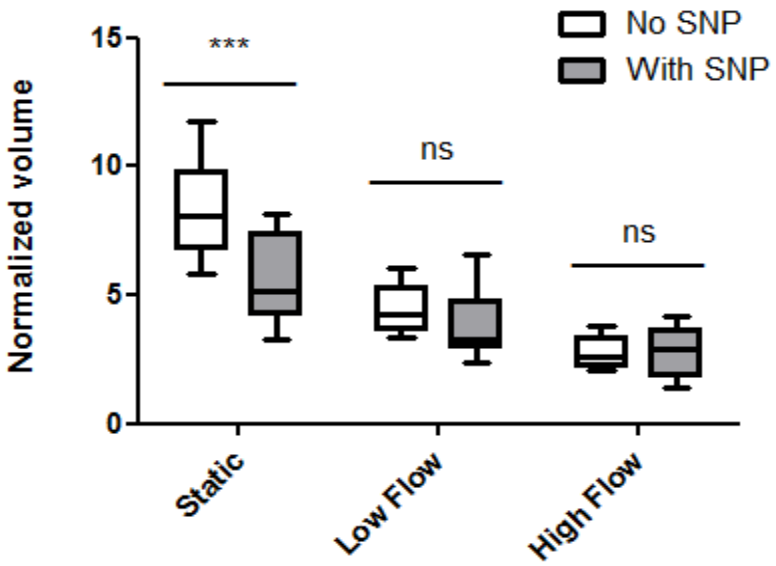

Figure 6. Quantification of the spheroids volume after 12 hours from the beginning of the experiment with and without the addition of SNP. For each spheroid, the calculated value was normalized for the volume measured at time zero. ***: P<0.0002, calculated using the unpaired student t-test.

3.3 Conclusions

In this chapter a new 3D model of breast cancer in which tumour spheroids of breast cancer cell lines has been designed and they are coupled with interstitial flow in a collagen I matrix.

The growing process of the spheroid for 12 hours was observed and quantified, identifying a differential effect of interstitial flow for the murine 4T-1 spheroids. Collective tumour cell migration was significantly modified by interstitial flow. In particular, interstitial fluid flow reduced the tumour growth and modified the hypoxic region of the tumour.

Moreover, we can further complicate the model, including a lymphatic endothelial compartment (LEC) in the spheroids (multicellular spheroids). In this way we could observe and quantify how LEC-tumour cell interaction in a biochemical relevant microenvironment influence breast cancer development.

3.4 References

[1] E.Senkus, F. Cardoso, and O. Pagani, *Time for more optimism in metastatic breast cancer?* Cancer Treat Rev, **40**, 220-228, 2014.

[2] S.J. Youngs, S.A. Ali, D.D. Taub and R.C. Rees, *Chemokines induce migrational responses in human breast carcinoma cell lines*, Int J Cancer, **71**, 257-266, 1997.

[3] B.N. Bidwell, C.Y. Slaney, N.P. Withana, S. Forster, Y. Cao, S. Loi, D. Andrews, T. Mikeska, N.E. Mangan, S.A. Samarajiwa, N.A. de Weerd, J. Gould, P. Argani, A. Möller, M.J. Smyth, R.L. Anderson, P.J. Hertzog and B.S. Parker, *Silencing of Irf7 pathways in breast cancer cells promotes bone metastasis through immune escape*, Nat Med, **18**, 1224-1231, 2012.

[4] J.G. Goetz, S. Minguet, I. Navarro-Lérida, J.J. Lazcano, R. Samaniego, E. Calvo, M. Tello, T. Osteso-Ibáñez, T. Pellinen, A. Echarri, A. Cerezo, A.J. Klein-Szanto, R. Garcia, P.J. Keely, P. Sánchez-Mateos, E. Cukierman and M.A. Del Pozo, *Biomechanical remodeling of the microenvironment by stromal caveolin-1 favors tumor invasion and metastasis*, Cell, **146**,148-163, 2011.

[5] V.Luga, L. Zhang, A. M. Viloria-Petit, A. A. Ogunjimi, M. R. Inanlou, E. Chiu, M. Buchanan, A. N. Hosein, M. Basik and J. L. Wrana, *Exosomes mediate stromal mobilization of autocrine Wnt-PCP signaling in breast cancer cell migration*, Cell, **151**, 1542-1556, 2012.

[6] S. Bayraktar, A.M. Gutierrez-Barrera, H. Lin, N. Elsayegh, T. Tasbas, J.K. Litton, N.K. Ibrahim, P.K. Morrow, M. Green, V. Valero, D.J. Booser, G.N. Hortobagyi and B.K. Arun., *Outcome of metastatic breast cancer in selected women with or without deleterious BRCA mutations*, Clin Exp Metastasis, **30**, 631-642, 2013.

[7] E.B. Voura, J.L. English, H.Y. Yu, A.T. Ho, P. Subarsky, R.P. Hill, C.V. Hojilla and R. Khokha, *Proteolysis during tumor cell extravasation in vitro: metalloproteinase involvement across tumor cell types*. PLoS One, **8**, e78413, 2013.

[8] K.J. Cheung, E. Gabrielson, Z. Werb and A. J. Ewald, *Collective invasion in breast cancer requires a conserved Basal epithelial program*, Cell, **155**, 1639-1651, 2013.

[9] K.V. Nguyen-Ngoc, K.J. Cheung, A. Brenot, E.R. Shamir, R.S. Gray, W.C. Hines, P. Yaswen, Z. Werb and A.J. Ewald, *ECM microenvironment regulates collective migration and local dissemination in normal and malignant mammary epithelium*, Proc Natl Acad Sci U S A, **109**, 2595-2604, 2012.

[10] M. Skobe, T. Hawighorst, D.G. Jackson, R. Prevo, L. Janes, P. Velasco, L. Riccardi, K. Alitalo, K. Claffey and M. Detmar, *Induction of tumor lymphangiogenesis by VEGF-C promotes breast cancer metastasis*, Nat Med, **7**,192-198, 2001.

[11] R.E. Nisato, J.C. Tille and M.S. Pepper, *Lymphangiogenesis and tumor* metastasis, Cell Tissue Res, **314**, 167-77, 2003.

[12] I. Crnic, K. Strittmatter, U. Cavallaro, L. Kopfstein, L. Jussila, K. Alitalo and G. Christofori, *Loss of neural cell adhesion molecule induces tumor metastasis by up-regulating lymphangiogenesis*,Cancer Research, **64**, 8630-8638, 2004.

[13] J. Xu, C. Zhang, Y. He, H. Wu, Z. Wang, W. Song, W. Li, W.He, S. Cai and W. Zhan, *Lymphatic endothelial cell-secreted CXCL1 stimulates lymphangiogenesis and metastasis of gastric cancer*, Int J Cancer, **130**, 787-797, 2012.

[14] S.M. Maula, M. Luukkaa, R. Grénman, D. Jackson, S. Jalkanen and R. Ristamäki, *Intratumoral lymphatics are essential for the metastatic spread and prognosis in squamous cell carcinomas of the head and neck region*, Cancer Res, **63**, 920-1926, 2003.

[15] P. Debinski, J. Dembowski, P. Kowal, T. Szydełko, A. Kołodziej, B. Małkiewicz, K. Tupikowski and R. Zdrojowy, *The clinical significance of lymphangiogenesis in renal cell carcinoma*, Med Sci Monit, **19**, 606-611, 2013.

[16] S.F. Schoppmann, B. Jesch, J. Zacherl, M. F. Riegler, J. Friedrich and P. Birner, *Lymphangiogenesis and lymphovascular invasion diminishes prognosis in esophageal cancer*, Surgery, **153**, 526-534, 2013.

[17] J. D. Shields, M.E. Fleury, C. Yong, A.A. Tomei, G. J. Randolph, and M. A. Swartz, *Autologous chemotaxis as a mechanism of tumor cell homing to lymphatics via interstitial flow and autocrine CCR7 signaling*, Cancer Cell, **11**, 526–538, 2007.

[18] W. J. Polacheck, J. L. Charest and R. D. Kamm, *Interstitial flow influences direction of tumor cell migration through competing mechanisms*, Proc Natl Acad Sci USA, **108**, 11115–11120, 2011.

[19] A. Issa, T.X. Le, A.N. Shoushtari, J.D. Shields, and M.A. Swartz, *Vascular endothelial growth factor-C and C-C chemokine receptor 7 in tumor cell-lymphatic cross-talk promote invasive phenotype*, Cancer Research, **69**, 349-357, 2009.

[20] M.E. Fleury, K.C. Boardman, and M.A. Swartz, *Autologous morphogen gradients by subtle interstitial flow and matrix interactions*, Biophys J, **91**, 113–121, 2006.

[21] S.M. Kakkad, M. Solaiyappan, B. O'Rourke, I. Stasinopoulos, E. Ackerstaff, V. Raman, Z.M. Bhujwalla and K. Glunde, *Hypoxic tumor microenvironments reduce collagen I fiber density*, Neoplasia, **12**, 608-617, 2010.

[22] C. Sahlgren, M.V. Gustafsson, S. Jin, L. Poellinger and U. Lendahl, *Notch signaling mediates hypoxia-induced tumor cell migration and invasion*, Proc Natl Acad Sci U S A, **105**, 6392-6397, 2008.

[23] D. Drasdo, and S. Hohme, *A single-cell-based model of tumor growth in vitro: monolayers and spheroids*, Phys Biol, **2**,133-147, 2005.

[24] R. Foty, *A simple hanging drop cell culture protocol for generation of 3D spheroids*, J Vis Exp, **51**, 2011.

[25] J. Friedrich, C. Seidel, R. Ebner and L.A. Kunz-Schughart, *Spheroid-based drug screen: considerations and practical approach*, Nat Protoc, **4**, 309-324, 2009.

[26] R. Senekowitsch-Schmidtke, K. Matzen, R. Truckenbrodt, J. Mattes, P. Heiss and M. Schwaiger, *Tumor cell spheroids as a model for evaluation of metabolic changes after irradiation*, J Nucl Med, **39**, 1762-1768, 1998.

[27] A. Ivascu, and M. Kubbies, *Rapid generation of single-tumor spheroids for high-throughput cell function and toxicity analysis*, Journal of Biomolecular Screening, **11**, 922-932, 2006.

[28] C.P. Ng and M.A. Swartz, *Fibroblast alignment under interstitial fluid flow using a novel 3-D tissue culture model,* Am J Physiol Heart Circ Physiol, **284**, 1771–177, 2003.

[29] M. Vinci, S. Gowan, F. Boxall, L. Patterson, M. Zimmermann, W. Court, C. Lomas, M. Mendiola, D. Hardisson and S.A. Eccles, *Advances in establishment and analysis of three-dimensional tumor spheroid-based functional assays for target validation and drug evaluation,* BMC Biol, **10**, 29, 2012.

[30] H. Dolznig, C. Rupp, C. Puri, C. Haslinger, N. Schweifer, E. Wieser, D. Kerjaschki and P. Garin-Chesa, *Modeling colon adenocarcinomas in vitro a 3D co-culture system induces cancer-relevant pathways upon tumor cell and stromal fibroblast interaction,* Am J Pathol, **179**, 487-501, 2011.

[31] F. Hirschhaeuser, H. Menne, C. Dittfeld, J. West, W. Mueller-Klieser and L.A. Kunz-Schughart, *Multicellular tumor spheroids: an underestimated tool is catching up again*, J Biotechnol, **148**, 3-15, 2010.

[32] C.P. Ng, C.L. Helm and M.A. Swartz, *Interstitial flow differentially stimulates blood and lymphatic endothelial cell morphogenesis in vitro,* Microvasc Res, **68**, 258-264, 2004.

[33] U. Haessler, J. C. M. Teo, D. Foretay, P. Renaud and M. A. Swartz, *Migration dynamics of breast cancer cells in a tunable 3D interstitial flow chamber,* Integr Biol, **4**, 401-409, 2012.

[34] S.A. DuPre, D. Redelman and K.W. Hunter, *The mouse mammary carcinoma 4T1: characterization of the cellular landscape of primary tumours and metastatic tumour foci*, Int J Exp Pathol, **88**, 351-360, 2007.

[35] P.B. Olkhanud, D. Baatar, M. Bodogai, F. Hakim, R. Gress, R.L. Anderson, J. Deng, M. Xu, S. Briest and A. Biragyn, *Breast cancer lung metastasis requires expression of chemokine receptor CCR4 and regulatory T cells*, Cancer Res, **69**, 5996-6004, 2009.

[36] H.M. Antonio, L.R. Mandarano, A.A. Coelho, M.G. Tiezzi, J.M. Andrade and D.G. Tiezzi, *Mouse renal 4T1 cell engraftment as a model to study the influence of hypoxia in breast cancer progression,* Acta Cir Bras, **28**, 142-147, 2013.

[37] Chaudary, N. and R.P. Hill, *Hypoxia and metastasis in breast cancer,* Breast Dis, **26**, 55-64, 2006.

[38] C.C. Wong, D.M. Gilkes, H. Zhang, J. Chen, H. Wei, P. Chaturvedi, S. I. Fraley, C.-M. Wong, U.-S. Khoo, I.O.-L. Ng, D. Wirtz, and G. L. Semenza, *Hypoxia-inducible factor 1 is a master regulator of breast cancer metastatic niche formation*, Proc Natl Acad Sci USA, **108**, 16369-16374, 2011.

[39] K. Sogawa, K. Numayama-Tsuruta, M. Ema, M. Abe, H. Abe, and Y. Fujii-Kuriyama, *Inhibition of hypoxia-inducible factor 1 activity by nitric oxide donors in hypoxia*, Proc Natl Acad Sci USA, **95**, 7368–7373, 1998.

Chapter 4

4.1 Overall conclusions

The control of the presentation of certain signals in three-dimensional space, has received extensive scientific interest and the ability to change and control the microenvironment and characterizing cellular response to several signals is a very relevant topic in many disciplines.

As stated in chapter 1, the purpose of the present thesis is the development of robust devices to control the cell microenvironment, in three dimensional biopolimeric gels, in terms of soluble factors and shear forces. In this work we proposed two different in vitro setups and their fabrication and testing have been important to obtain a realistic characterization of cellular response to several microenvironmental stimulation.

First, we developed a microfluidic device for the culture of mammalian cells, subjected to linear gradient of biomolecular factors. Our goal was to make up a device as stable as possible thus to allow to achieve a high degree of consistency in the experimental procedure. Technical issues, such hydrogel stability, local heterogeneities within the gel and gas-liquid separation of the culturing media were addressed. Easy and cheap strategy to solve them in a systematic fashion were highlighted.

In addition, we presented in 3D matrix a novel, integrated 3D model of murine breast cancer spheroids, with tunable interstitial flow. The interstitial flow can be decisive in influencing the first step of the metastasis process of murine breast cancer, which is characterized by a collective type of migration. In particular collective tumour cell migration was significantly modified by interstitial flow reducing the tumour growth.

4.2 Future Directions

In this work we presented methods for the design, fabrication and testing of microfluidic devices for controlling cell microenvironment in terms of soluble factors and shear stress how single stimulations. However many type of cells in vivo are constantly exposed to various stimuli simultaneously. Thus there is a need to regulate the combination of several signals to evaluate their additive, synergistic, antagonist, or non interacting effects. The control of multiple stimuli such as biochemical and mechanical, in an *in vitro* microsystem is especially important for optimization of microenvironments in tissue engineering applications and tumour progression where the combination of more signals may occur.

In the contest of tumour progression the mechanism by which tumour cells integrate these signals to leave the original site tumour and invade new tissue remain poorly understood. As described in chapter 1 the tumour cells, that express cytokine receptor and secrete the cognate cytokines, in the presence of interstitial fluid can generate its own peri-cellular gradients. It would be interesting to evaluate how peri-cellular gradient of cancer cells, created in the presence of interstitial flow, can alter the composition of cell environment and can recruit several cells types including fibroblast, lymphatic endothelial cells and other type of cells presented in the surrounding microenvironment.